A FINITE DIFFERENCE MODEL OF CHANNEL WAVES IN A COAL SEAM

by

W.H.Darken

T 1729

A Thesis submitted to the Faculty and the Board of Trustees of the Colorado School of Mines in partial fulfillment of the requirements for the degree of Master of Science in Geophysics.

Signed: William H. Darken
William H. Darken

Golden, Colorado
Date: April 17, 1975

Approved: Frank A. Hadsell
Frank A Hadsell
Thesis Advisor

George V. Keller
George V. Keller
Head of Department

Golden, Colorado
Date: April 17, 1975

ABSTRACT

Based on algorithms established by Leitinger (1969), a program has been written which can calculate the complete displacement vector anywhere in a horizontally-layered medium with azimuthal symmetry, given a point-source excitation. The program utilizes the finite difference technique. This program made possible the study of a high-amplitude disturbance in a coal seam, the energy of which was trapped within the seam by a high acoustic impedance contrast at the seam's boundaries. This disturbance is called a 'channel wave'. The modeled media consisted of a thin coal seam bounded above and below by competent shale. The output was a time series of horizontal and vertical displacements at selected locations in the model, including a line of stations along the length of the coal seam. Output data indicated that a strong channel wave was formed, with the possibility that its energy decreased linearly with distance from the source. Discussions of ray and mode analysis are included, and these are shown to be in agreement with the calculated data.

CONTENTS

ILLUSTRATIONS

INDEX OF SYMBOLS

km	kilometers
m	meters
ms	milliseconds
$\Delta r, \Delta z$	radial and vertical increment between grid points of the finite difference model
s,sec	seconds
Δt	time increment from one cycle of finite difference calculations, to the next
v_c, v_s	compressional and shear velocity

ACKNOWLEDGMENTS

The author wishes to express his sincere gratitude to Professor Frank A. Hadsell of the Colorado School of Mines, who acted as his advisor on this research project. Professor Hadsell's enthusiasm for the finite difference method was instrumental in developing the finite difference program on which most of this thesis is based, and it was also Professor Hadsell's idea to apply it to the interesting coal seam problem His many discussions and patient explanations are most deeply appreciated.

I am grateful to Professor Maurice W. Major for encouraging a look into the model aspects of channel waves, and for his interpretations of the synthetic records.

To the office of Geochemistry and Geophysics of the United States Geological Survey goes my sincere appreciation for funds which used to pay for the many hours of computer time required.

Finally, I wish to thank the Office of the Graduate School at the Colorado School of Mines, which provided the numerous extensions of computer time necessary for the developement of the finite difference program.

INTRODUCTION

The presence of channel waves in thin coal seams has been observed and investigated analytically by T.C. Krey (1963). The nature of these waves is similar to that of acoustic waves travelling along a speaking tube in a ship It is hoped that they may be made useful in the mining of coal

Channel waves are caused by the containment of elastic wave energy - if a formation is bounded above and below by lithologies which cause large contrasts in density and wave speeds, then energy within the seam tends to remain within the seam Channel waves are not to be confused with Stoneley or other boundary waves Coal seams can be particularly good media for channel waves: they are often thin, bounded by competent rock, and generally of low velocity and density.

Our chief interest in channel waves lies in the hope that they can aid in mapping discontinuities in coal beds It would significantly assist a mining company in making an economic evaluation if the boundaries of a coal bed could be detected by dispersed or reflected channel waves. Locating faults would also be of importance in planning mining operations. Locating cavities due to previous mining operations would be of concern to a miner stripping off the overburden And the detection of channel deposits would be a matter of safety to deep-rock miners .

The specific purpose of this thesis is to generate channel waves by a computer modeling technique, and to observe the character of the waves. Especially important is the amplitude, as a large amplitude would indicate that energy is effectively trapped within the seam The modeling technique that was used was the method of finite differences.

Alterman and Karal (1968) have taken an equation of motion for displacement in a homogeneous, isotropic medium, and they have written the component

differential equations in their finite difference form. Using these equations, and the example of a program written by Leitinger (1969), a computer program has been developed which can output displacements, for any selected set of points, due to a point source, anywhere in a horizontally-layered, homogeneous, isotropic medium. This program, FDNL.F10, will be used to find the time-history of displacement in and about a coal seam embedded in competent shale

THE PROGRAM

Equations and algorithms used in the program FDNL.F10 come directly from Alterman and Karal (1968). This reference treats the finite difference method incorporated in FDNL.F10 thoroughly. Only basic concepts and unique characteristics of the program will be described here.

The finite difference method can be represented, in a general sense, as an approximate, numerical, solution of a differential equation. This solution is obtained by replacing the analytic derivative operators in the differential equation by operators which can be programmed for a computer. An example of the method, as applied to a first and second order derivative, is given in figure 1.

The purpose of FDNL.F10 was to apply this technique to the equation of motion for a homogeneous, isotropic, elastic medium (figure 2), so that the displacement at a point in a new time frame could be described in terms of displacement at a set of points in the previous time frames. Figure 3a gives the equation of motion, in cylindrical coordinates, for radial displacement. Figure 3b gives the finite difference scheme derived from the equation in figure 3a, using the operators shown in figure 1.

Finite difference equations can also be derived for the transformation of displacements across boundaries (Alterman and Karal, 1968), and this allows the model to be layered. For reasons of computational efficiency, FDNL.F10 was limited to horizontal boundaries.

As can be inferred from figure 3b, a displacement calculation at a point (m,n) at time p+1 requires displacements from nine points in time frame p, and one point (m,n) in time frame p-1. This requires that the computer store all displacements for all points for the previous two time frames p and p-1, to calculate displacements for the new time frame p+1. This is the single biggest

FINITE DIFFERENCE PROCEDURE

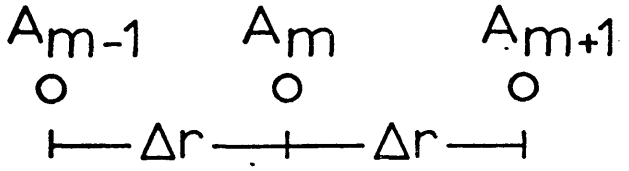

$$\left.\frac{\partial A}{\partial r}\right|_m = \frac{A_{m+1} - A_{m-1}}{2(\Delta r)}$$

$$\left.\frac{\partial^2 A}{\partial r^2}\right|_m = \frac{(A_{m+1} - A_m) - (A_m - A_{m-1})}{(\Delta r)^2}$$

Figure 1. An example of the finite difference procedure. A_i is the displacement at point i, and Δr is the distance between points i and i+1.

FOR A HOMOGENEOUS, ISOTROPIC, ELASTIC MEDIUM

$$\rho \frac{\partial^2 \bar{u}}{\partial t^2} = (\lambda + 2\mu)\nabla(\nabla \cdot \bar{u}) - \mu \nabla \times \nabla \times \bar{u}$$

Figure 2. The equation of motion for a homogeneous, isotropic, elastic medium. Lambda and mu are the Lame coefficients, rho is density, t is time, and u is a displacement vector.

$$\left[\frac{\partial^2 A}{\partial r^2} + \frac{1}{r}\frac{\partial A}{\partial r} - \frac{1}{r^2}A + \frac{\partial^2 B}{\partial r \partial z}\right] + \frac{v_s^2}{v_c^2}\left[\frac{\partial^2 A}{\partial z^2} - \frac{\partial^2 B}{\partial r \partial z}\right] = \frac{1}{v_c^2}\frac{\partial^2 A}{\partial t^2}$$

Figure 3a. One of two equations of motion used, in cylindrical coordinates. A is the radial displacement function, B is the vertical displacement function, r is the radial distance from the origin, z the vertical distance, t is time, and v_c and v_s are the compressional and shear velocities.

$$\begin{aligned} A_{m,n,p+1} = {} & 2A_{m,n,p} - A_{m,n,p-1} + \left[\frac{v_c \Delta t}{\Delta r}\right]^2 \left[A_{m+1,n,p} - 2A_{m,n,p} + A_{m-1,n,p}\right] \\ & + \frac{1}{2}\left[\frac{v_c \Delta t}{\Delta r}\right]^2 \frac{1}{m}\left[A_{m+1,n,p} - A_{m-1,n,p}\right] - \left[\frac{v_c \Delta t}{\Delta r}\right]^2 \frac{1}{m^2} A_{m,n,p} \\ & + \frac{1}{4}\left[\frac{v_c \Delta t}{\Delta r}\right]^2 \left[\frac{\Delta r}{\Delta z}\right]\left[1 - \frac{v_s^2}{v_c^2}\right]\left[B_{m+1,n+1,p} - B_{m+1,n-1,p}\right. \\ & \left. - B_{m-1,n+1,p} + B_{m-1,n-1,p}\right] \\ & + \left[\frac{v_c \Delta t}{\Delta r}\right]^2 \left[\frac{\Delta r}{\Delta z}\right]^2 \left[\frac{v_s^2}{v_c^2}\right]\left[A_{m,n+1,p} - 2A_{m,n,p} + A_{m,n-1,p}\right] \end{aligned}$$

Figure 3b. The finite difference scheme for radial displacement, as derived from the equation in figure 3a. The variables in 3a are redefined as $r = m\Delta r$, $z = n\Delta z$, and $t = p\Delta t$, where Δr and Δz are incremental lengths along the r and z axes, and Δt is an increment in time. From Alterman and Karal (1968).

storage requirement of the computer.

Also, it may be observed in figure 3b that a displacement calculation at a point requires displacements from the eight points which surround it, in a rectangular grid system. This scheme clearly fails at any boundary, since a point is not surrounded by points with similar physical properties. The edge of a layer coincident with the model's axis of symmetry (the vertical axis on which the point source lies) can be dealt with by taking advantage of the symmetry. Alterman and Karal (1968) have developed equations for this circumstance. Displacement on the edges of a layer coincident with the free surface or another layer are found with the application of the usual boundary conditions: stresses vanish at the free surface, and stresses and displacements are continuous across layer interfaces. An explicit solution with these conditions requires that a fabricated overlap be added to one of the layers at a boundary, and stability criteria require that this overlap be added to the layer with the lower velocity. Figure 4 illustrates this.

Treatment at the bottom and outer edge of the model remains unsatisfactory. Calculation of displacements is done out to but not including these perimeter points. This means that all calculations are done with the restriction that these points are held rigid, which is equivalent to fastening these edges of the model to a perfectly rigid wall. This produces unwelcome, strong reflections which travel back into the interior of the model, and interfere with the displacements of interest. It seems reasonable that a practical solution exists to this problem; electrical engineers are able to arrange the input impedance of a long transmission line such that it appears to be an infinite conductor, thus eliminating reflections of electromagnetic energy, and an analogous solution may exist here. One approach has been made by Lysmer and Kuhlemeyer (1969). Their solution was to give the boundary a viscous property such that it would absorb impinging waves; however, it was designed for a steady-state system and would require significant modification to handle the range of frequencies generated by the

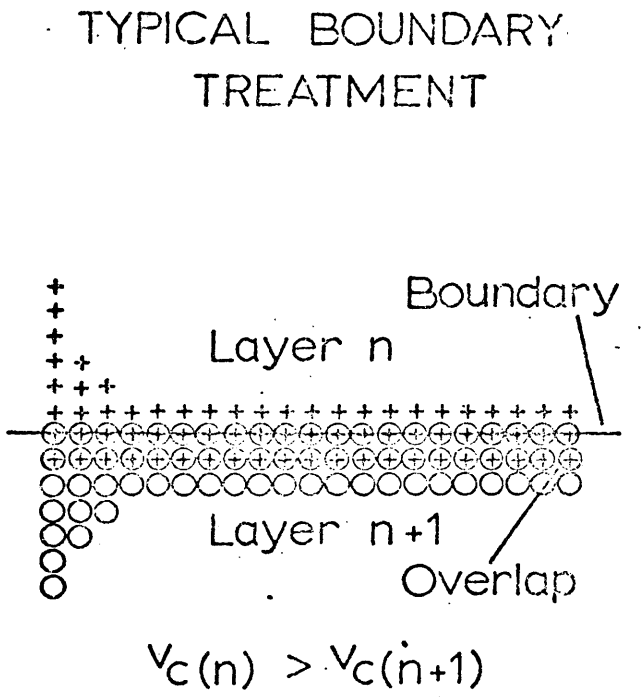

Figure 4. The addition of the 'imaginary' row of grid points at a layer boundary.

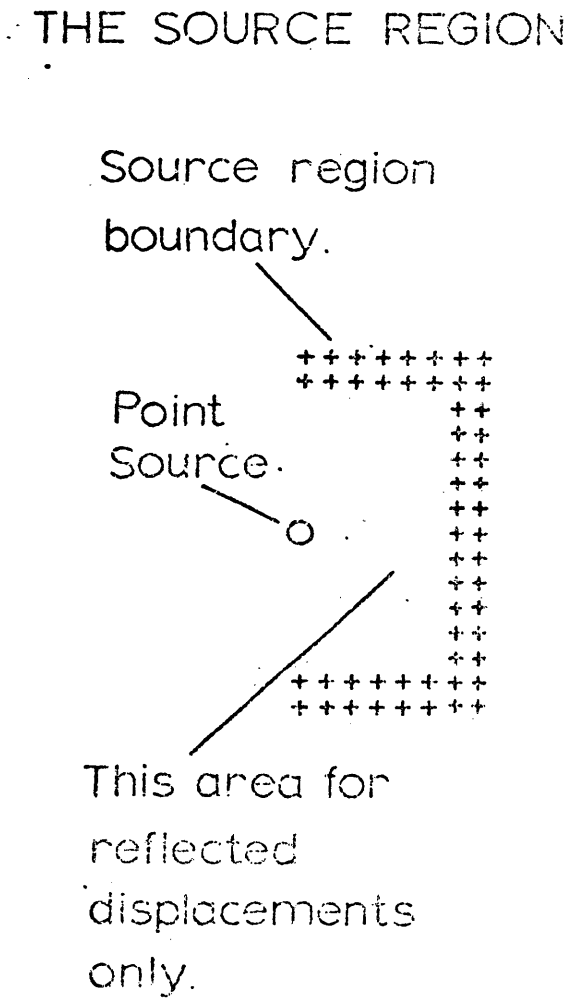

Figure 5. A simplified view of the source region.

transient pulse in FDNL.F10.

The finite difference method breaks down if displacements differ grossly between adjacent grid points. In a physical model, this would correspond to exceeding the elastic limits of the propagating medium; in the finite difference model the problem which arises is one of round-off errors, dependent on the computer's word length. This issue becomes most acute in the proximity of the point source, since as one approaches the source the energy density increases as the squared reciprocal of the distance. The solution used in FDNL.F10 is from Alterman and Karal (1968), and utilizes a 'source region'. Within the source region the finite difference method is not used to propagate displacements directly due to the point source, but the method is used to propagate reflections arriving from the rest of the model. Displacement due to the source is calculated analytically at the perimeter of the region, and is allowed to pass only outwards from the source region. Figure 5 illustrates the source region.

The parameters of the geologic model (figure 6) are input layer by layer. Each layer has assigned to it a compressional velocity, a shear velocity, a density, and a thickness. Common to all layers are a vertical space increment, Δz, a radial space increment, Δr, and total horizontal extent. The space increments determine the grid of discrete points which sample the geologic model. This two-dimensional grid is suggested by figure 7. The selection of the time increment between displacement calculations is not a trivial matter. Too large an increment leads to large, oscillating instabilities in the calculations, and too small an increment wastes valuable computer time. Alterman and Karal (1968) give criteria which determine an upper bound for the time increment.

The output for the model consists of displacements at selected grid points, which are saved in an output file as the program calculates from one time instant to the next. As a matter of convenience, these points where displacements are saved will be identified as geophones.

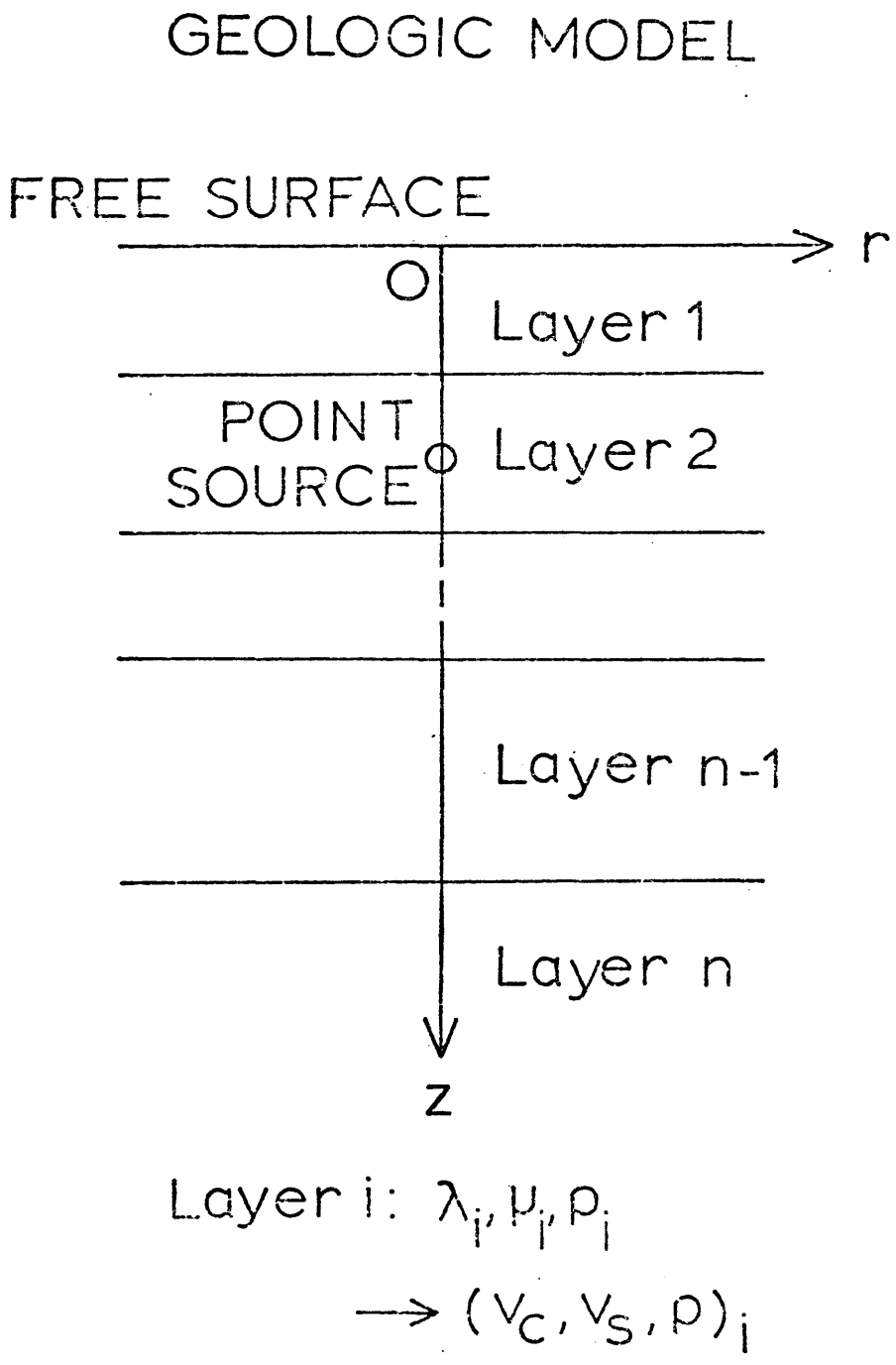

Figure 6. An example of a geologic model. The Lame coefficients lambda and mu, describing the physical properties of layer i, are redefined in terms of the compressional and shear velocities.

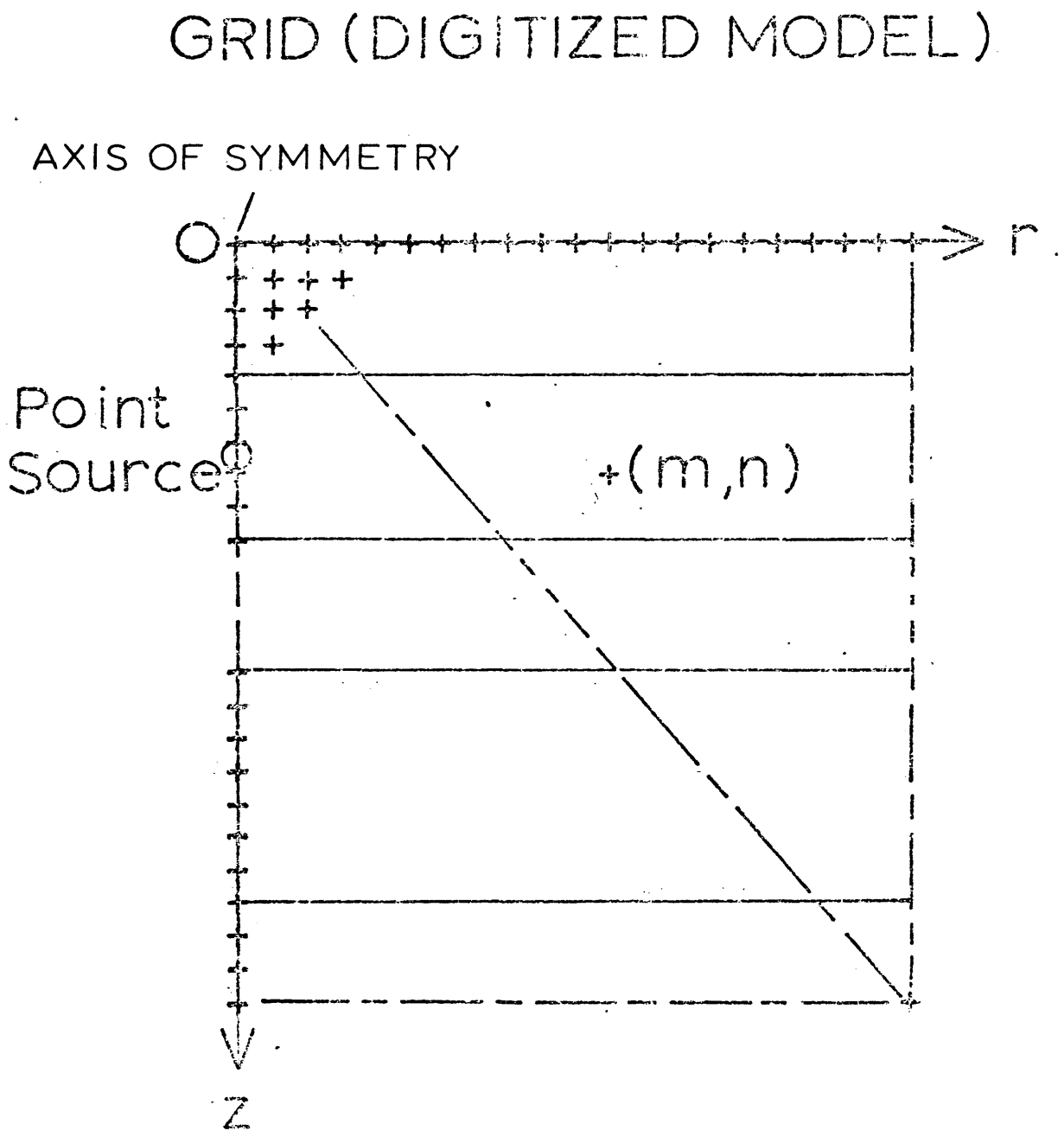

Figure 7. The digitized geologic model of figure 3. Each discrete point is identified by a pair of indices (m,n). Because of azimuthal symmetry, only half of the total model need be considered.

The salient features of FDNL.F10 are that (1) it can treat an arbitrary number of layers; (2) the sequence of layer velocities is immaterial - a low velocity layer may precede or antecede any higher velocity layer; (3) the source may be placed in any layer. The only restriction on physical characteristics of adjacent layers is that a positive compressional velocity contrast must always be accompanied by a positive shear velocity contrast. This restriction precludes what is generally regarded as an unusual situation, especially in exploration seismology, and is not a serious handicap to the program.

Note that the ability of the program to calculate displacements for an arbitrary number of modeled layers enables the user to submit a large model simply by dividing it into many thin layers, only one of which must occupy the core of the computer at any given time.

Leitinger's program ran a model of 11,500 grid points for 500 time cycles on a CDC 6400 computer, and its computation time was approximately forty minutes. The same program, modified to run on a PDP 10, required sixty-four minutes for a model of 9520 grid points and 625 time cycles. FDNL.F10, run on a PDP 10, required seven hours (420 minutes) for a model of 29,610 grid points and 790 time cycles.

TESTING THE PROGRAM

To ensure confidence in the results obtained with FDNL.F10, the program was tested for several simple cases. Two important tests are described below.

Case I

This model was run in order to give the program a simple test, and to compare results to a similar model run by Leitinger (1969). The model consists of a layer over a half-space, in which the acoustic velocities and density of the half-space are set to zero. This creates a situation in which a slab is bounded above and below by a free surface, and if a point source is placed in the center of the slab, one can expect that displacements measured at symmetrical points on the two surfaces should be equal. The test was merely to check that these displacements are indeed equal.

Parameters used for the model are listed in Table 1.

The source pulse used for the test is shown in figure 8. Results are shown in figures 9a,9b,9c, and 9d. The reader should compare 9a with 9c, and 9b with 9d. Correcting for the mirror-image relationship of the vertical displacements, it can be seen that the curves are a good match. The minor differences are explained by the slightly different way in which the two boundaries are handled in the program (the free surface is treated in a different manner than the other layer boundaries). The curves are an excellent match to Leitinger's; the peak-to-peak excursion at the epicenter matches Leitinger's to four places.

Case II

This model is based on one of Leitinger's (1969) more complex runs. Unlike the previous model, there is no self-consistency check on the output, and the test consisted of comparing FDNL.F10 output with the output which Leitinger obtained.

Physically, the model represents a low velocity material between two

Table 1

Parameters input to FDNL.F10 for Case 1

Number of time increments: 200
Number of layer: 4
Number of vertical grid lines: 110
Radial space increment: 500 m
Vertical space increment: 500 m
Time increment: 0.5 sec
Amplification factor for source: 1.0
Depth of source: 10000 m

Layer	Layer Thickness(m)	v_c(m/sec)	v_c(m/sec)	ρ(gm/cc)
1	5000	600	400	3.0
2	10000	600	400	3.0
3	5000	600	400	3.0
4	1500	0	0	0.0

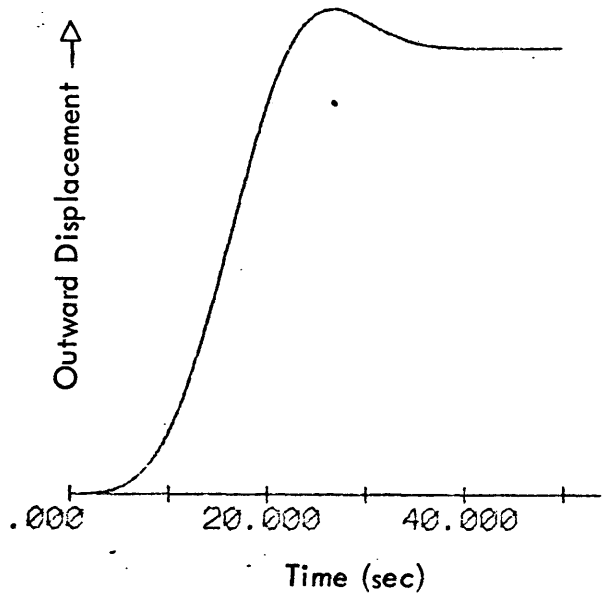

Figure 8. The source pulse for Case I in terms of displacement at the perimeter of the source region.

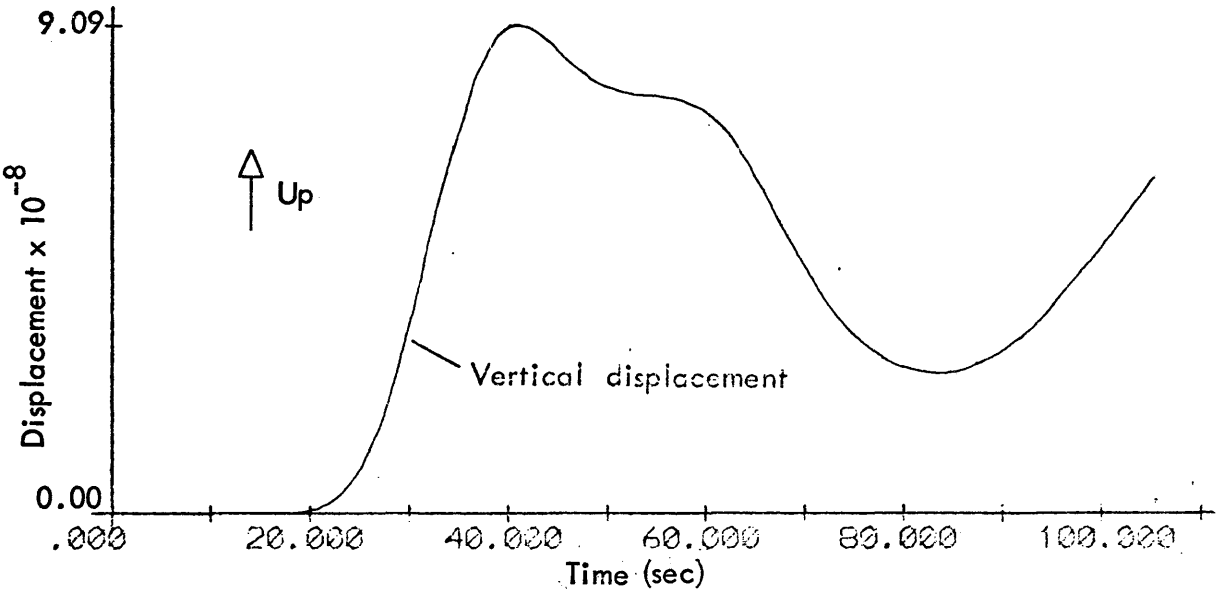

Displacement at the epicenter.

Figure 9a.

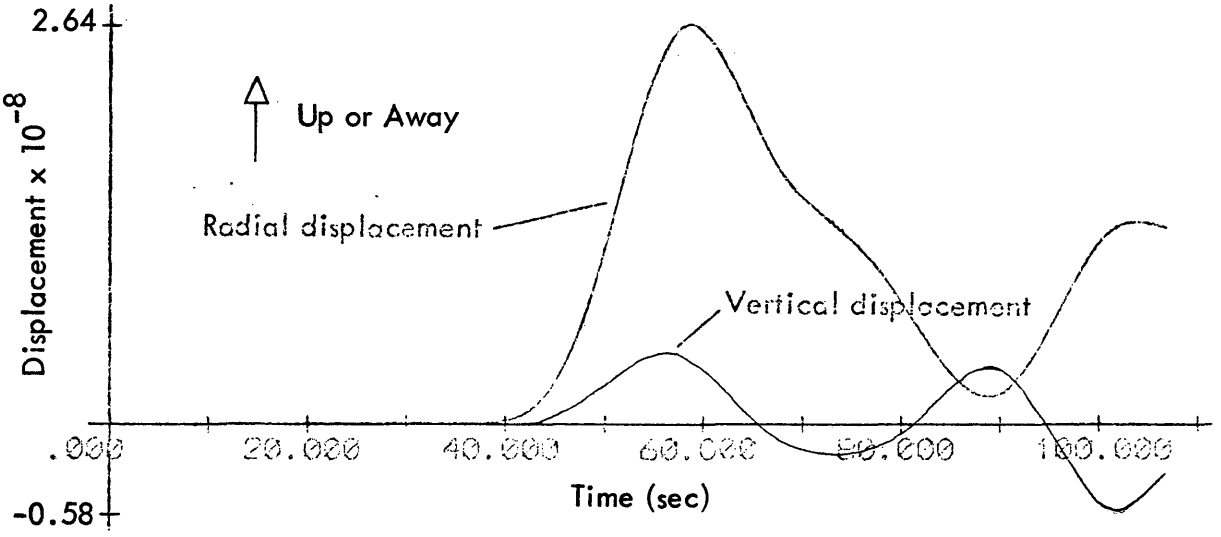

Displacement at a radial distance of two source depths, on the free surface.

Figure 9b.

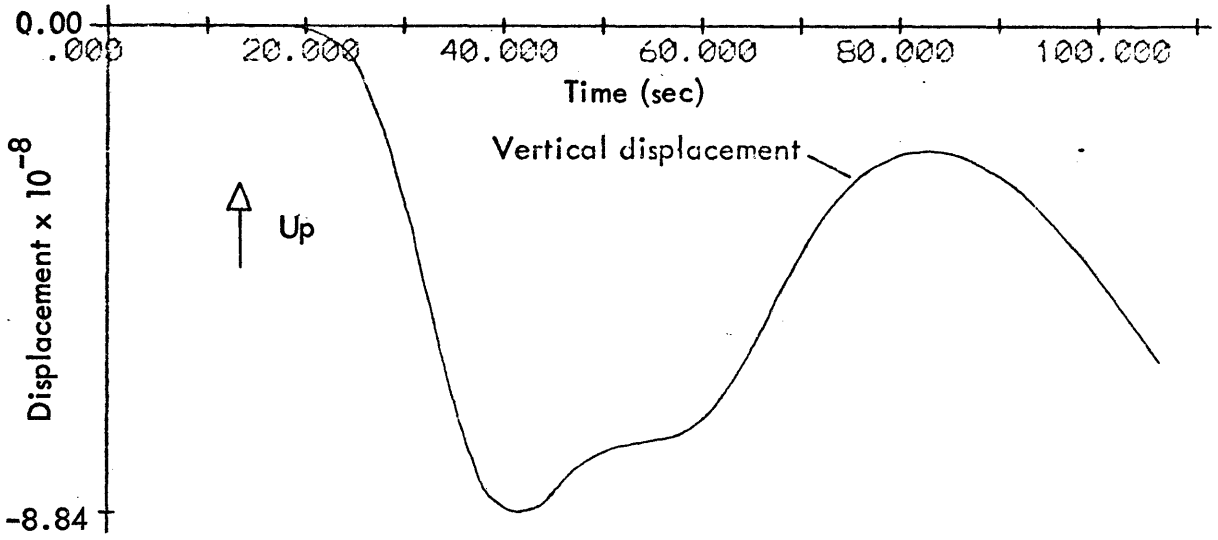

Displacement directly below the epicenter, at the base of the slab.

Figure 9c.

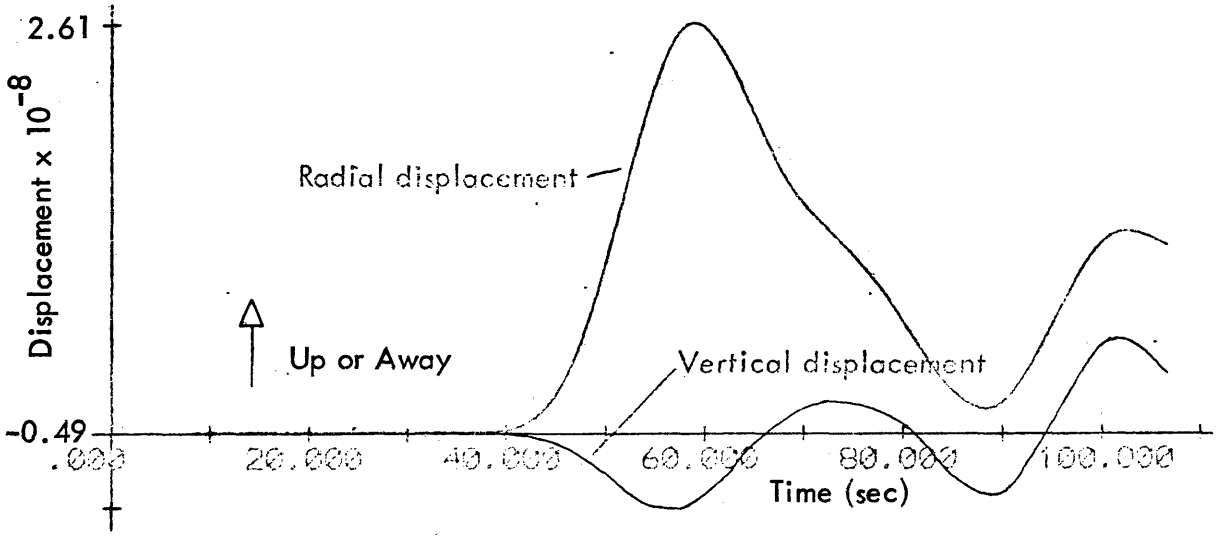

Displacement at a radial distance of two source depths, at the base of the slab.

Figure 9d.

higher velocity materials. It was felt that this model would indicate whether the program was properly handling the two different types of boundary conditions (going from high to low velocity media, and going from low to high velocity media). Also, the ability of the program to efficiently run a multi-layered model would be given a good test.

The input parameters of Leitinger and for FDNL.F10 are given in Table 2.

The source pulse is shown in figure 10. The output is given in figures 11a, 11b, and 11c. These compare excellently with the results of Leitinger, except for the last several seconds where effects of the model edge interfere (Leitinger evidently ran a larger-sized model, and did not get this interference). For comparison, some of Leitinger's results are shown in figure 12.

The difference in shear wave velocities for the bottom layer did not seem to affect the results significantly.

The successful completion of this test was regarded as final evidence that FDNL.F10 functioned properly.

Table 2

Input parameters for Case II

Leitinger's parameters:

Layer 1: v_c = 6.0 km/sec
v_s = 4.0 km/sec
ρ = 3.0 gm/cc
Thickness = 30 km

Layer 2: v_c = 5.5 km/sec
v_s = 3.0 km/sec
ρ = 3.0 gm/cc
Thickness = 5 km

Layer 3: v_c = 8.0 km/sec
v_s = 4.5 km/sec
ρ = 4.5 gm/cc
Thickness = half space

Depth of source: 8.0 km
Length of step-like pulse: 6.0 sec

FDNL.F10 parameters:

Number of time increments: 260
Number of layers: 6
Number of vertical grid lines: 110
Radial space increment: 1000 m
Vertical space increment: 1000 m
Time increment: 1.5 sec
Amplification factor for source: 1.0
Depth of source: 8000 m

Layer	Layer Thickness(m)	v_c(m/sec)	v_s(m/sec)	ρ(gm/cc)
1	20000	6000	4000	3.0
2	10000	6000	4000	3.0
3	5000	5500	3000	3.0
4	20000	8000	4000	4.5
5	20000	8000	4000	4.5
6	20000	8000	4000	4.5

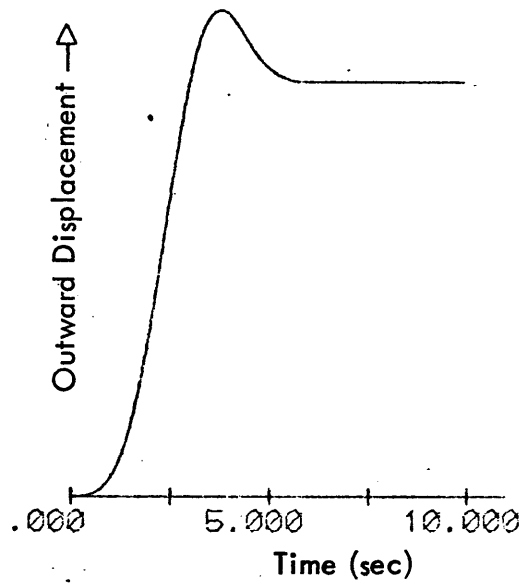

Figure 10. The source pulse for Case II in terms of displacement at the perimeter of the source region.

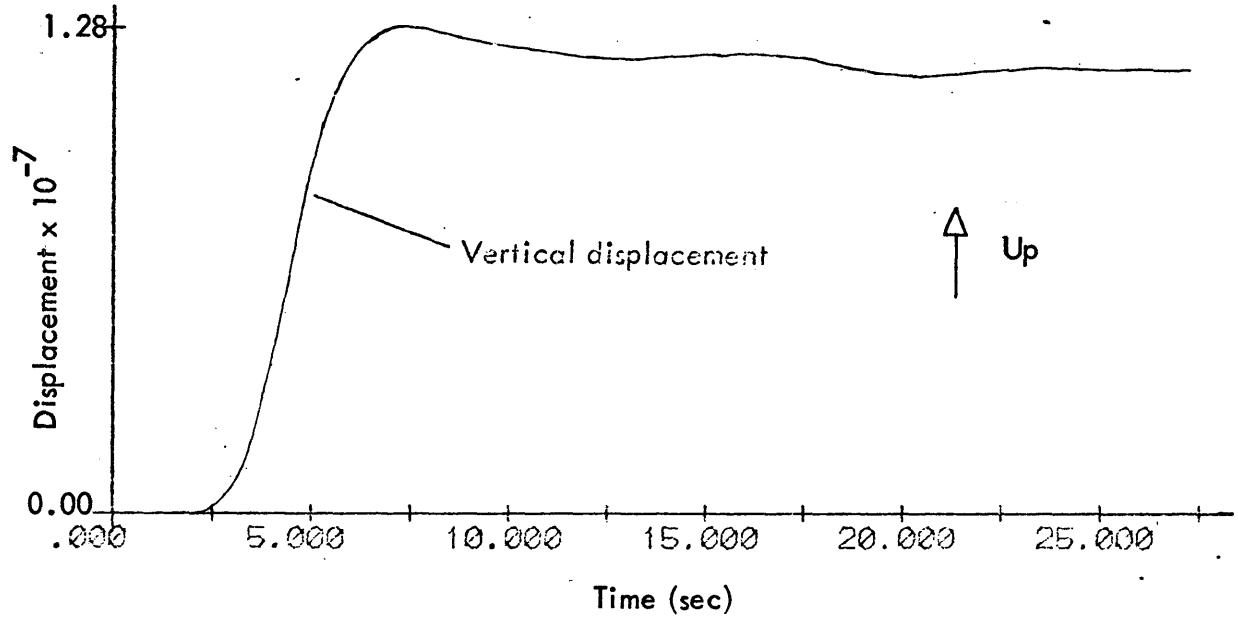

Figure 11a. Displacement at the epicenter.

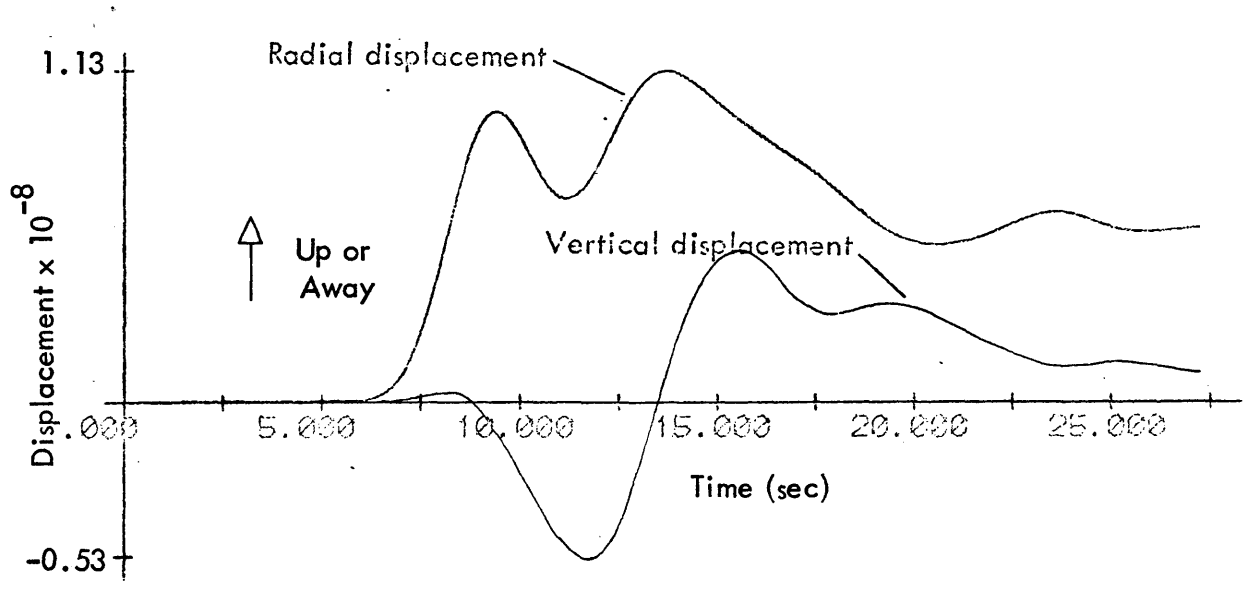

Figure 11b. Displacement at a radial distance of four source depths, at the free surface.

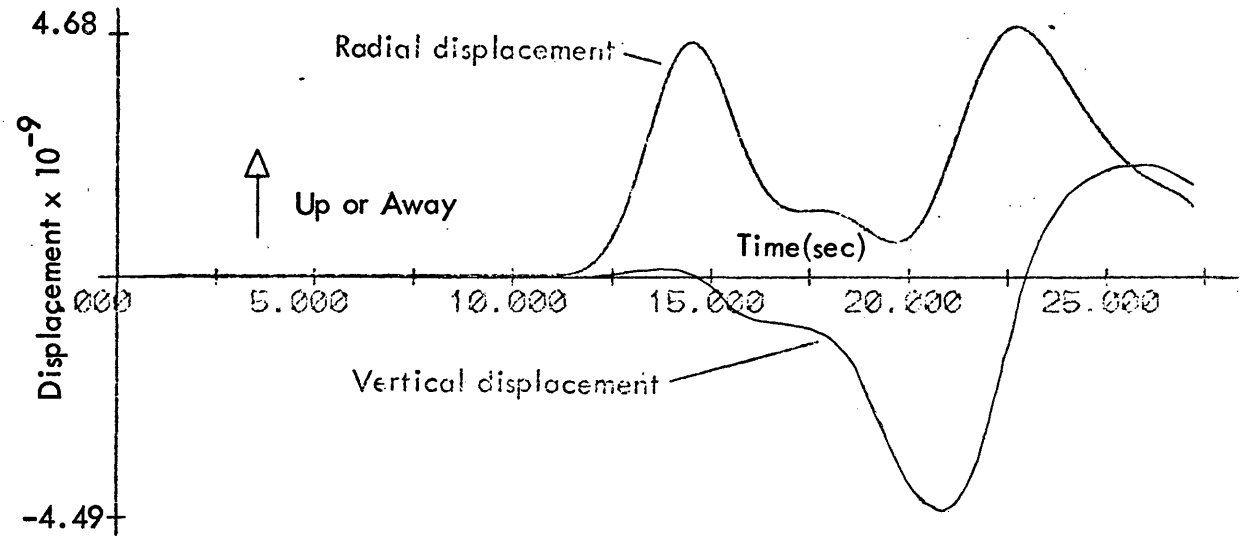

Figure 11c. Displacement at a radial distance of eight source depths, at the free surface.

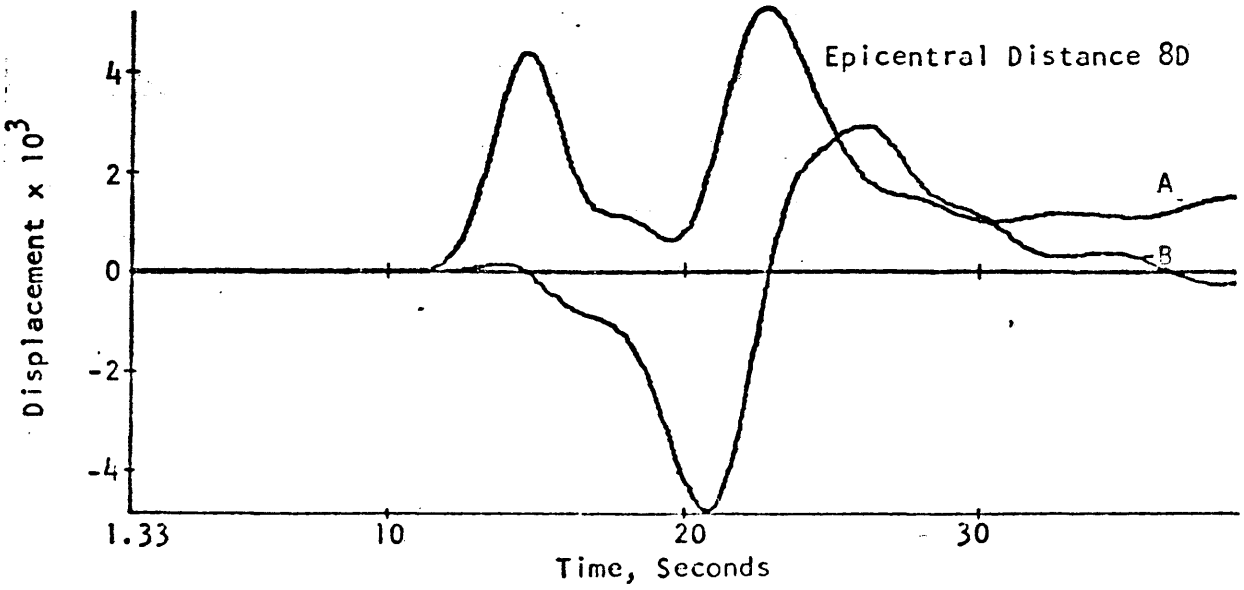

Figure 12. Leitinger's results at a radial distance of eight source depths, at the free surface. To be compared with figure 11c.

DESCRIPTION OF THE COAL SEAM MODEL

The geologic model of interest is shown in figure 13. A thin coal seam, 3 m thick, is overlain by 30 m of shale, and itself overlies 30 m of shale. Each layer is 56 m in horizontal extent, measured from the axis of symmetry. Above the top layer of shale is a free surface, and below the bottom layer of shale is the base of the model - a rigid wall which necessarily appears here and at the outer perimeter of the model. In the center of the coal seam, on the axis of symmetry, is the compressional point source. The model, for all practical purposes, may be considered to be in the shape of a cylinder; because of azimuthal symmetry only two displacements lying in any plane determined by the symmetry axis and a radius need be calculated. These are, of course, radial and vertical displacements.

The numerical values assigned as rock parameters are from Krey (1963). This is in spite of the prejudice that Poisson's ratio for coal does not equal 0.25 (this was used to relate shear velocity to compressional velocity). Schwaitzer (1965) seriously disputes Krey's value for the compressional velocity of coal (1200 m/sec), claiming that it is closer to 2300 m/sec. Other evidence indicates that the properties of coal vary over a wide range.

The source wavelet, as it would exist 0.4 m from the source, is given in figure 14a. Its shape at 1.6 m is given in figure 14b. It's a modification of the pulse used by Leitinger (1969), in that it is the derivative of his step-like pulse. This gave the pulse a shape more like that from an explosion. The equation for the pulse used is given in figure 15.

Figures 14a and 14b show that the initial source pulse rapidly becomes a doublet, as the far-field terms assume dominance. The peak period of the wavelet (in the far field) is about 2 ms; this was felt to be a sharp pulse, with a comfortable margin for sampling (the sampling interval was 0.07 ms).

GEOLOGIC MODEL

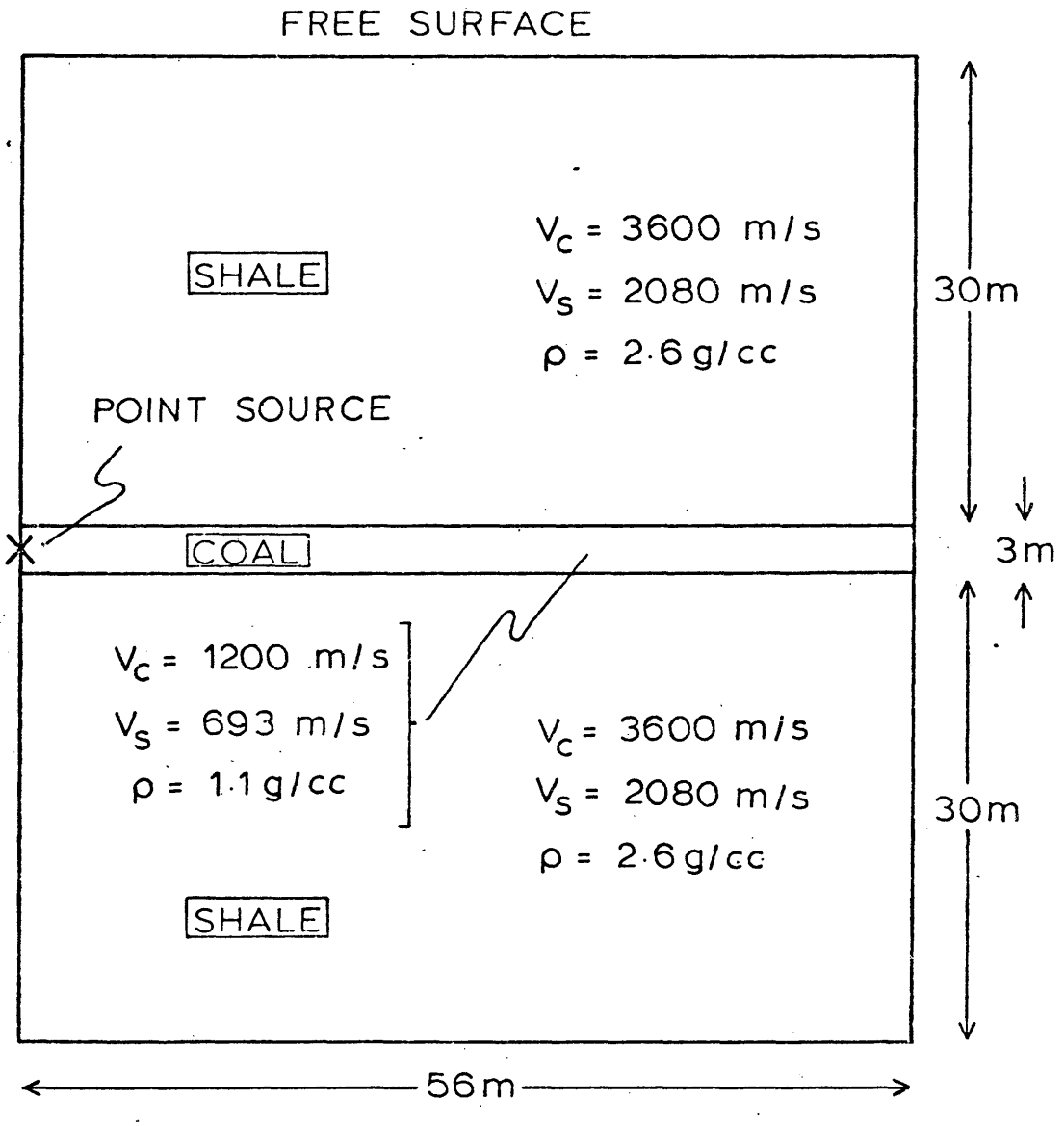

Figure 13. The geologic model of interest.

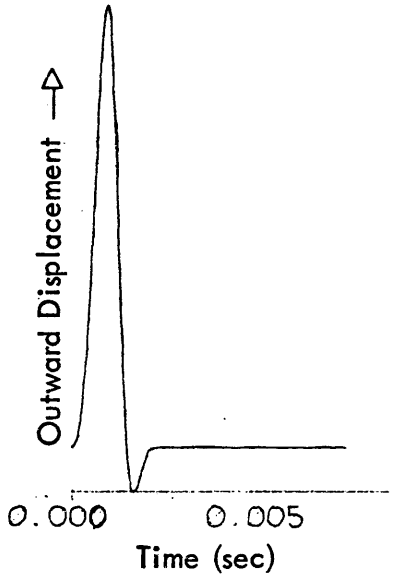

Figure 14a. The source pulse in terms of displacement, 0.4 m from the source.

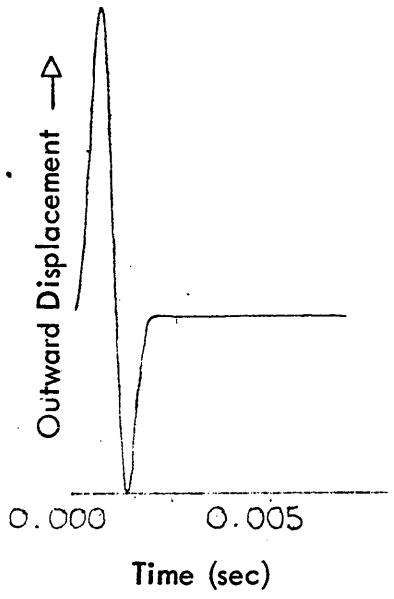

Figure 14b. The source pulse in terms of displacement, 1.6 m from the source.

DISPLACEMENT AT TIME t AND DISTANCE r =

$$c_1F_1(t) + c_2F_2(t) - 4c_1F_1(t-\Delta) - 4c_2F_2(t-\Delta) + 6c_1F_1(t-2\Delta) + 6c_2F_2(t-2\Delta) - 4c_1F_1(t-3\Delta) - 4c_2F_2(t-3\Delta) + c_1F_1(t-4\Delta) + c_2F_2(t-4\Delta)$$

$$c_1 = \frac{1}{3\Delta^3 r^3} \qquad c_2 = \frac{1}{\Delta^3 r^2 v_c}$$

$$F_1(t) = (t - \frac{r}{v_c})^3 \qquad F_2(t) = (t - \frac{r}{v_c})^2$$

Δ - SOURCE WIDTH PARAMETER

v_c - COMPRESSIONAL VELOCITY IN SOURCE LAYER

Figure 15. The equation of the source pulse. The source width parameter has dimensions of time, and its value corresponds to approximately 1/4 the width of the source pulse.

From the dispersion curves in Krey (1963), it is possible to estimate the group velocity of the Airy phases of the channel wave. For the first mode this turns out to be approximately 1000 m/sec, with a wavelength of approximately 15 m. This yields a period of 15 ms. The radius of the model was selected mainly on the basis of this Airy phase. With a radius of 56 m, and a projected model run time of 56 ms, the first mode Airy phase would have developed to a sufficient degree to be analyzed, but would have calculations terminated before this Airy phase was reflected at the model's edge. Since the model is only 56 m in radius, a compressional wave in shale whose velocity is 3600 m/sec can travel to the boundary of the model in only 15.6 ms. Thus we can expect to find some spurious reflections from the edges of the model mingled with the waves of interest. This was not found to be a serious problem.

RUNNING THE MODEL

Figure 16 shows the model in the form used by FDNL.F10. The input parameters are listed in Table 3.

A qualification of the parameters in Table 3 is that due to an internal problem of the computer, the program ran for only 488 time cycles, a serious departure from the hoped-for 800 cycles.

The size of the vertical space increment was determined by the thickness of the coal seam: the minimum number of points that would adequately model the coal seam in a vertical direction was arbitrarily chosen to be ten, and 3.0 m/10 increments = 0.3 m/increment. Testing showed that a radial increment of 0.4 m could be used without seriously affecting results. After the selection of these parameters, the choice of the maximum time increment was forced by Alterman and Karal's stability criteria. The value used was 0.00007 sec.

Because of the limited computer core size, the number of vertical grid columns was a tradeoff between minimizing the number of model layers, and maximizing the number of grid columns. A minimum number of layers being desirable as this decreased the required computer time. (only one layer could be held in the core area at any given time, and it was time-consuming to shuffle layers from disk to core). The number of layers chosen was seven, six for the two shale units, and one for the coal seam.

The total time for which wave displacements were calculated is (488-1) cycles x 0.00007 sec/cycle = 0.03409 sec. The lag time between initial source excitation and arrival of the first wave at a boundary (the time at which the program begins finite difference calculations) is 0.00114 sec. The last displacement is then calculated at (0.03409 + 0.00114) sec = 0.03523 sec, from the time the source is activated.

If the Airy phase of the channel wave travels at 1000 m/sec (see Krey,

FINITE DIFFERENCE MODEL

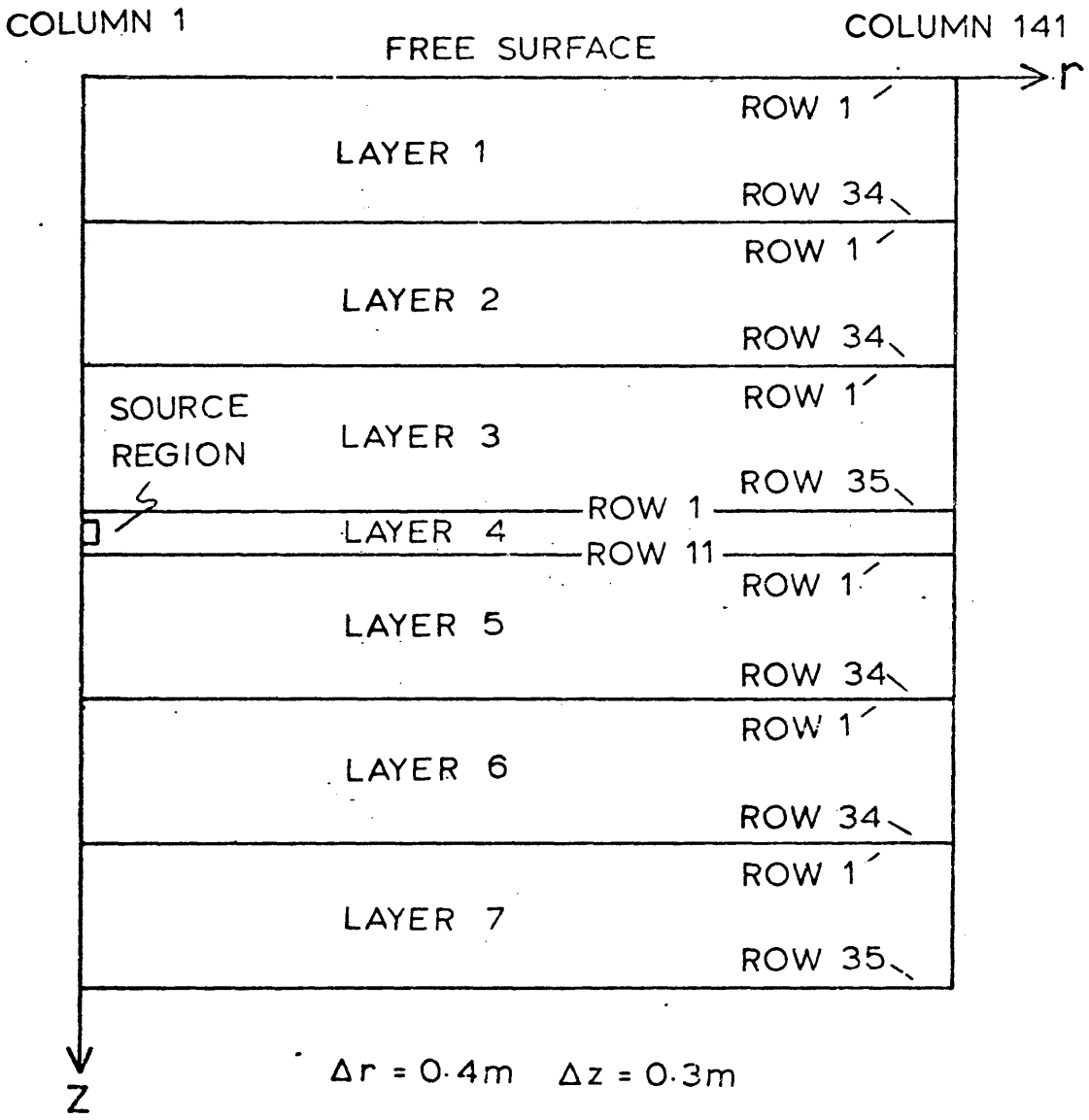

	V_c(m/s)	V_s(m/s)	ρ(g/cc)
LAYERS 1,2,3,5,6,7	3600	2080	2·6
LAYER 4	1200	693	1·1

Figure 16. The model as input to FDNL.F10.

Table 3.

The input parameters for the coal seam model:

Number of time increments: 800
Layer in which source is placed: 4
Half-height of source region: 3
Number of layers: 7
Number of vertical grid columns: 141
Radial space increment: 0.4 m
Vertical space increment: 0.3 m
Time increment: 0.00007 sec

Layer	Index Units	Thickness(m)	v_c (m/sec)	v_s (m/sec)	ρ (gm/cc)
1	34	9.9	3600	2080	2.6
2	34	9.9	3600	2080	2.6
3	35	10.2	3600	2080	2.6
4	11	3.0	1200	693	1.1
5	34	9.9	3600	2080	2.6
6	34	9.9	3600	2080	2.6
7	35	10.2	3600	2080	2.6

Indices of geophones (the first index is the grid column, the second the grid row):

1,1		1,90	1,95	1,100	5,105	1,112
		26,90	26,95	26,100	26,105	26,112
51,1	51,51	51,90	51,95	51,100	51,105	
		76,90	76,95	76,100	76,105	
101,1		101,90	101,95	101,100	101,105	
		126,90	126,95	126,100	126,105	
140,1		140,90	140,95	140,100	140,105	

1963), then this part of the channel wave shall have travelled 35.2 m by the end of computations. Thus, there should be no reflections of this phase from the model's edge.

Figure 17 indicates the positions of all the geophones in the model. In the program, each geophone has a pair of indices which identifies its position; the first index is the vertical grid column, and the second is the horizontal grid row. This is the way their positions are indicated in figure 17. Essentially, there are five rows of geophones. One is on the free surface, three are in the shale immediately above the coal seam, and one is slightly off-center within the coal seam. A geophone is placed at indices (51,51) to give a vertical string of six geophones, and geophones at (1,112) and (26,112) are placed to give a check on the symmetry of displacement about the coal seam (these geophones are in positions symmetrical to geophones at (1,100) and (26,100)). The geophone positions within the coal seam were selected so that a comparison could be made with output from a finite element program (Oden, 1972). This program is to be run on the CDC 7600 at the University of California at Berkeley.

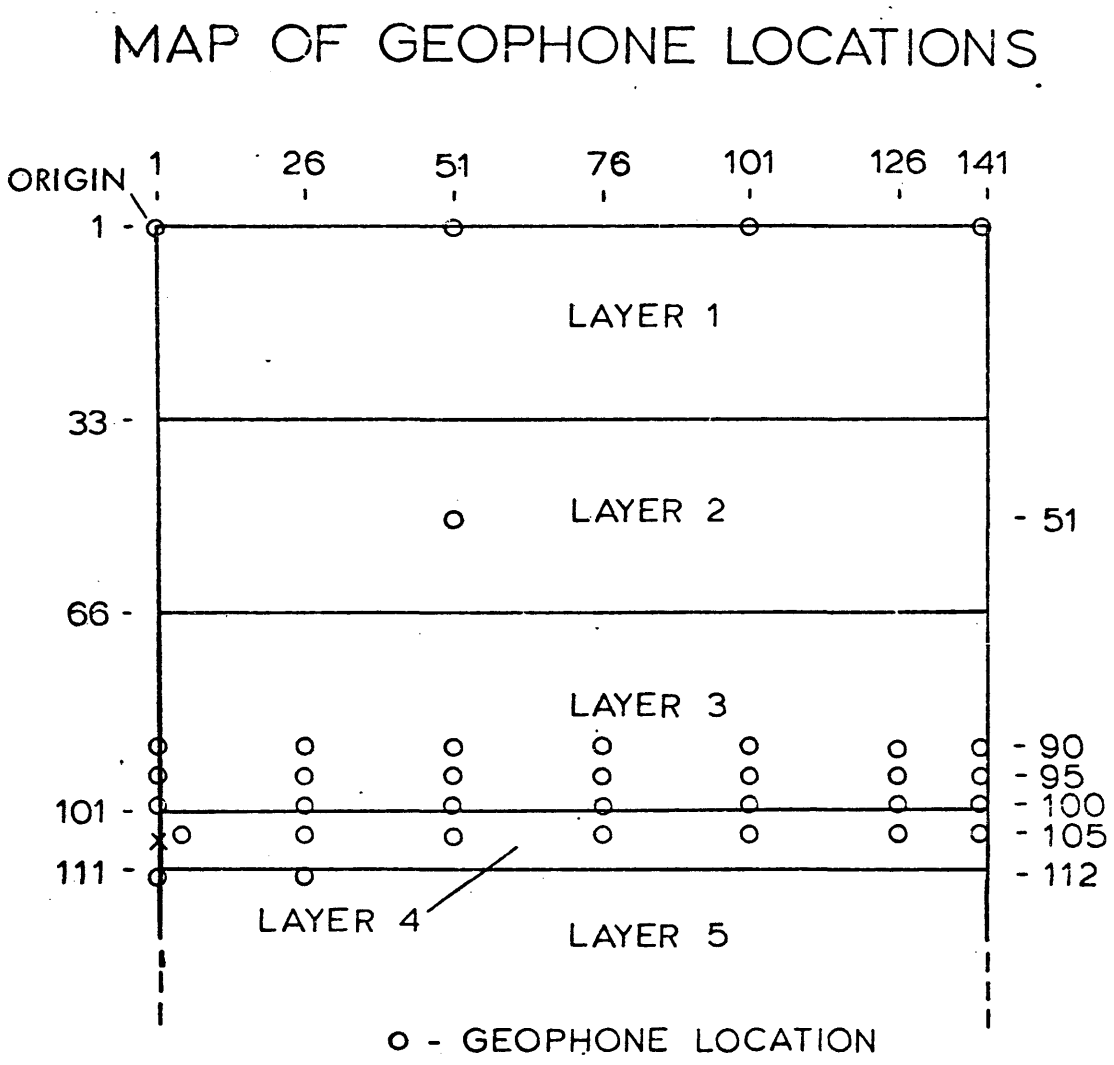

Figure 17. The location of all geophones in the model. The numbers along the top of the model refer to the grid column, and the numbers along the sides refer to the grid row. Radial distance from the origin = (grid column - 1) x 0.4 m; vertical distance from the origin = (grid row - 1) x 0.3 m.

RESULTS FROM THE COAL SEAM MODEL

General Comments

Output from FDNL.F10 includes a radial and vertical displacement for each geophone, for each time increment. These numerical results are bulky, and are not included in this thesis. The output as presented here is in four types of plotting formats: (1) an individual geophone has its radial and vertical displacements plotted together to the same scale, with positive vertical displacement being up (towards the free surface); (2) the radial or vertical traces of a group of geophones are plotted one above the other, each trace normalized to its maximum and minimum, so that changes may be observed along a radial or vertical alignment of geophones, with positive vertical displacement being down (away from the free surface); (3) a variation on (2) in that all traces are normalized to the same displacement, so that the true relative amplitude is preserved between traces; (4) a variation on (2) in that the amplitude of a trace is proportional to the square root of its distance from the source.

For formats (2), (3), and (4) there is over each trace an ordered pair of numbers; the first is the maximum displacement for that trace, and the second is the minimum. They are intended as an aid in comparing traces. Also, for these formats, the time scale does not begin at 0.00 sec, but is offset to 0.00114 sec. The distance between tic marks is still 0.0025 sec (2.5 ms).

Henceforth, each geophone will be referred to by its metric coordinates, the first coordinate being the radial distance, in meters, from the axis of symmetry, and the second being the depth, in meters, from the free surface.

The maximum amplitude of the source pulse used in the coal seam model was arbitrarily set to 1.0. This value yielded acceptable records (computer roundoff errors were not apparent, to a noticeable degree, and sufficient

energy was released). This amplitude has not been related to the energy of the source, although, using Sharpe's (1942) theory and other source parameters, the total radiated elastic energy could be computed. Thus numbers describing amplitudes have no meaningful units, and are to be compared only with each other.

A comment must be made which applies to much of the output. Two plots in format (1) are given for the geophone (0.0,0.0) in figures 18a and 18b. The first figure indicates a high frequency wave beginning approximately at 0.0325 sec (A). The second shows a complete history of a high frequency transient beginning approximately at 0.012 sec (B) and ending at 0.025 sec (C). These high frequency waves are due to an instability which evidently began at the epicenter (0.0,0.0) for reasons which are still a puzzle. The second instability (A) has such great amplitude that the first instability (B) cannot be seen on the same trace. When the later portion of this trace was muted and the amplitude renormalized, the first instability became apparent. If the reader looks closely, he can see part of the 'real' waveform immediately preceding the first instability. The great amplitude of these instabilities made it necessary to excise the later portions of several records, in order that the instability did not obscure the interesting waves. The muting problem was most severe with the traces nearest to (0.0,0.0).

A warning should be sounded with regard to the traces recorded on grid column 140. This column is located one increment from the outer edge of the model; immediately after the arrival of a true wave directly from the source or from a real reflection, a strong, false, reflection will arrive from the model edge. This reflection will be almost out of phase with the impinging wave, and will have the effect of almost differentiating the actual waveform.

A Note Regarding Mode Theory

A plot of the particle displacements at the free surface, figure 19,

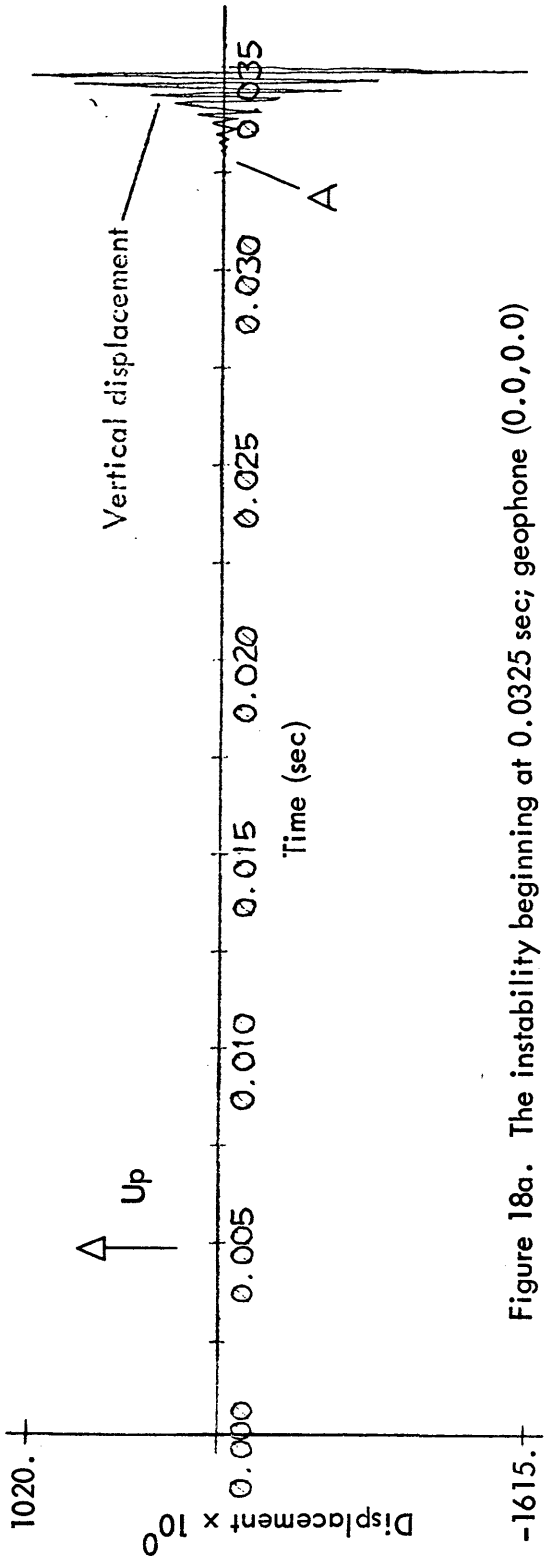

Figure 18a. The instability beginning at 0.0325 sec; geophone (0.0,0.0)

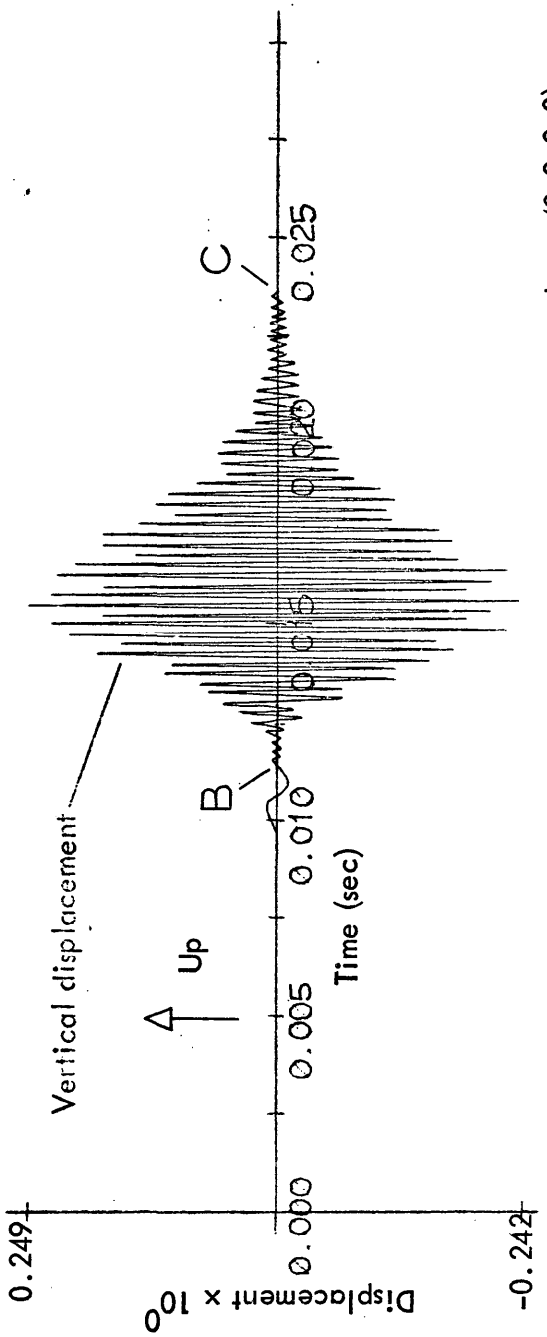

Figure 18b. The instability beginning at 0.012 sec; geophone (0.0,0.0)

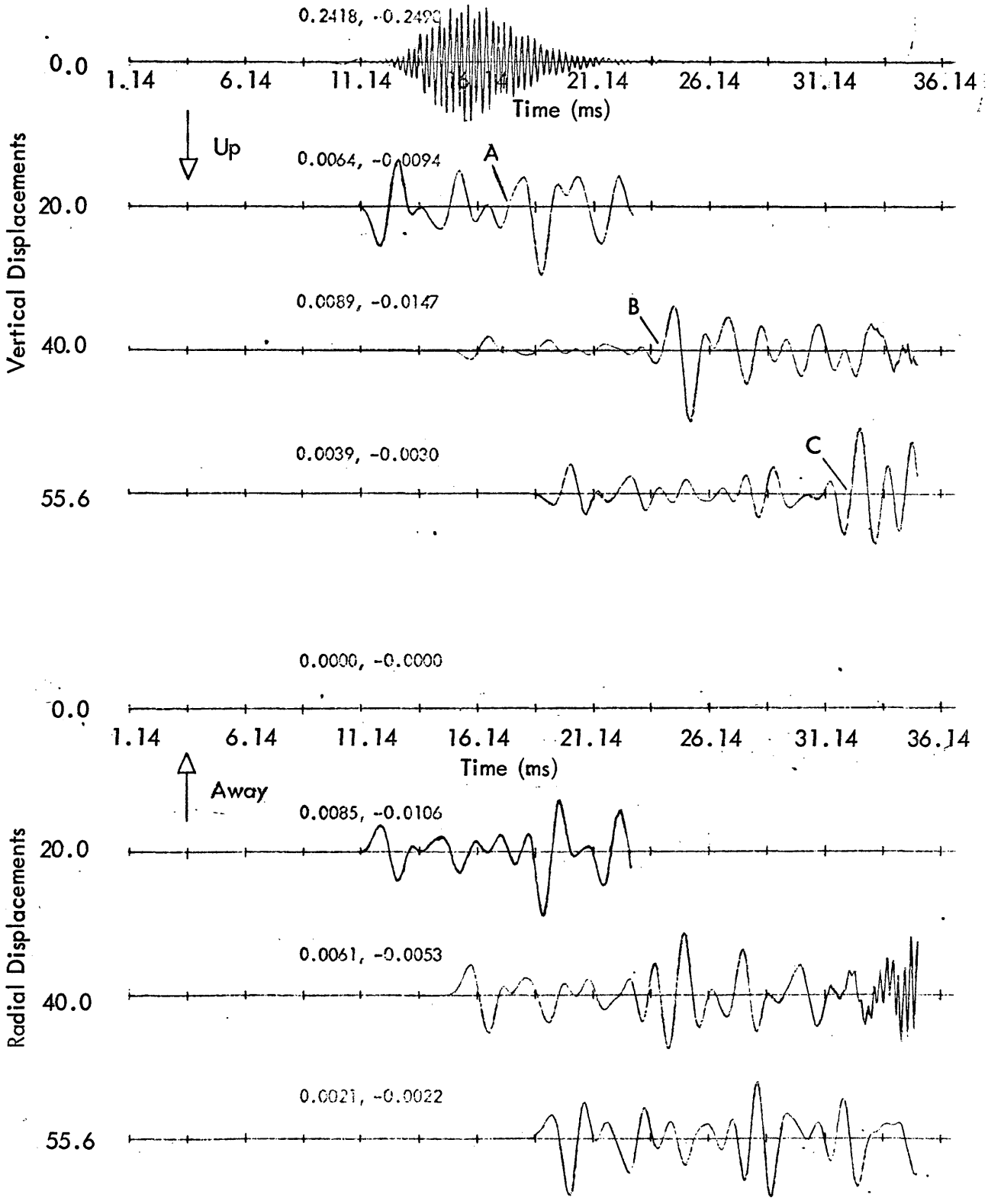

Figure 19. The geophones on the free surface; format (2). Tic mark separation is 2.5 ms. Distance from the axis of symmetry is noted to the left of each trace.

indicates a very strong phase arriving at the times given below.

Indices	Arrival Time(sec)
(20.0,0.0)	0.018(A)
(40.0,0.0)	0.024(B)
(55.6,0.0)	0.032(C)

There is a strong inclination to call this phase the surface wave. However, the apparent velocity between (20.0,0.0) and (40.0,0.0) is 3100 m/sec. This speed would give a seismologist pause before calling this disturbance a Rayleigh wave, as its velocity across the free surface exceeds the velocity of the shear body wave (2080 m/sec).

Listed below are the calculated arrival times of energy traveling as a compressional wave from the source to the upper shale-coal interface, there converting to a shear wave and as such traveling to the free surface.

Indices	Arrival Time(sec)
(20.0,0.0)	0.0185
(40.0,0.0)	0.0252
(55.6,0.0)	0.0314

There is a good correlation between the shear arrival and the apparent surface wave. The observation to be made is that here the "surface wave" consists predominantly of the PS arrival. As a generalization, in the epicentral region the line between body waves and surface waves is a fine one and it is enrealistic to expect classical mode analysis to be strictly valid. It is noteworthy that for the phase above, the apparent velocity between (40.0,0.0) and (55.6,0.0) is 2100 m/sec and this is more in line with a surface wave velocity.

As this is the reader's first opportunity to examine the output, he will be encouraged to see that the first breaks arrive when expected, the first motion

is up for the vertical component, and away for the radial. Also, vertical amplitude increases from 20 to 40 meters; this is consistent with PS propagation, as at 40 meters the rays are more parallel to the radial direction, and transverse displacement is more parallel to the Z-direction. These observations give confidence that things are occuring as they should be.

A Check on the Program

As mentioned previously, geophones were placed symmetrically above and below the coal seam, as a partial check on the program. Figure 20a is a plot of the displacements 0.3 m above the seam, on the axis of symmetry, and figure 20b is a plot of displacements 0.3 m below the seam, on the axis of symmetry. As is apparent, the displacements are near-perfect mirror images of each other until 18 ms (A), when reflections arrive from the top and bottom of the model (these have dissimilar boundaries). Figures 21a and 21b give the output for geophones at locations which are 10 m from the axis of symmetry and 0.3 m above and below the coal seam. The radial displacements are equal and the vertical displacements mirror images, until reflections arrive from the top and bottom of the model at 18 ms (A).

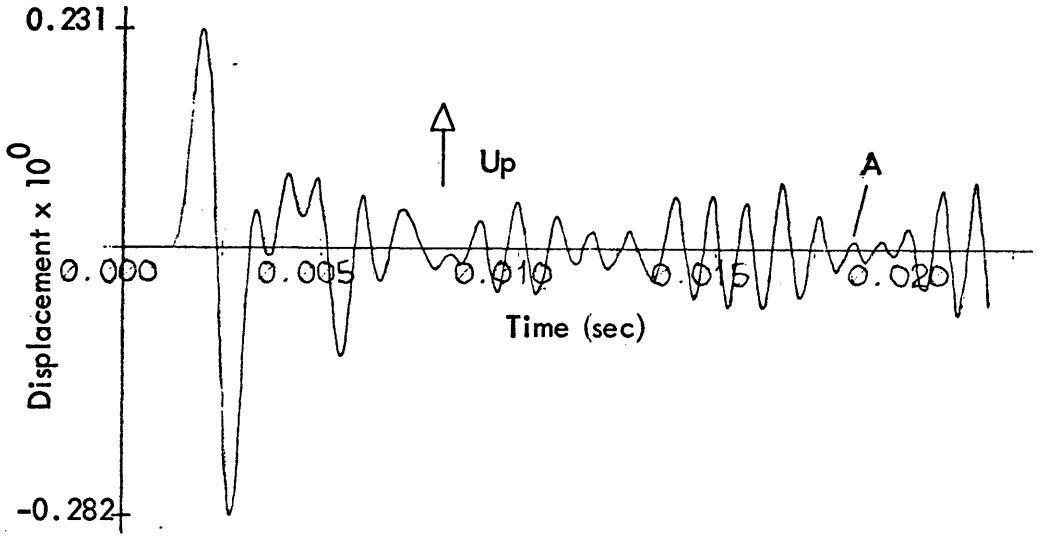

Figure 20a. Vertical displacement on the axis of symmetry, 0.3 m above the coal seam.

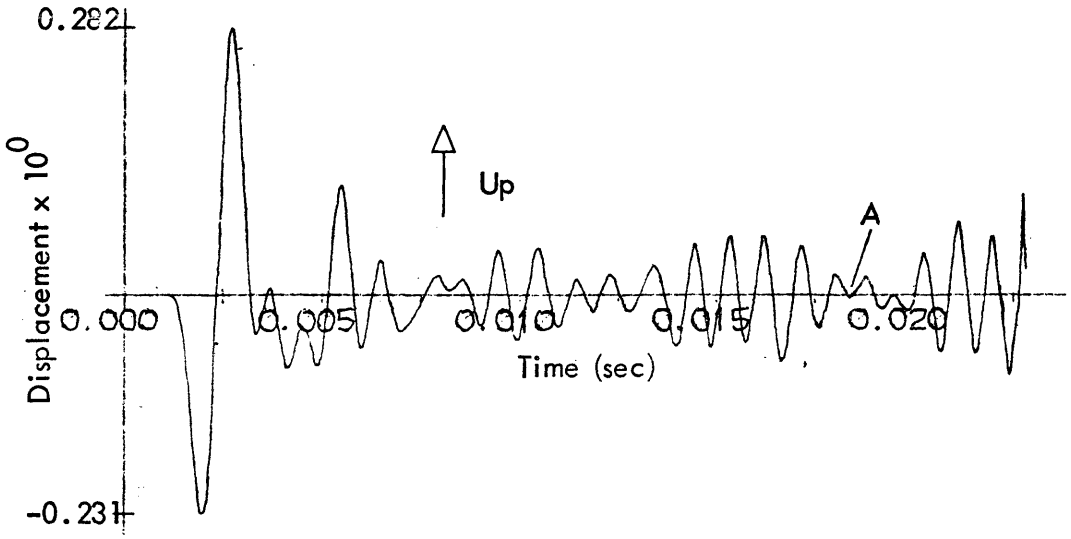

Figure 20b. Vertical displacement on the axis of symmetry, 0.3 m below the coal seam.

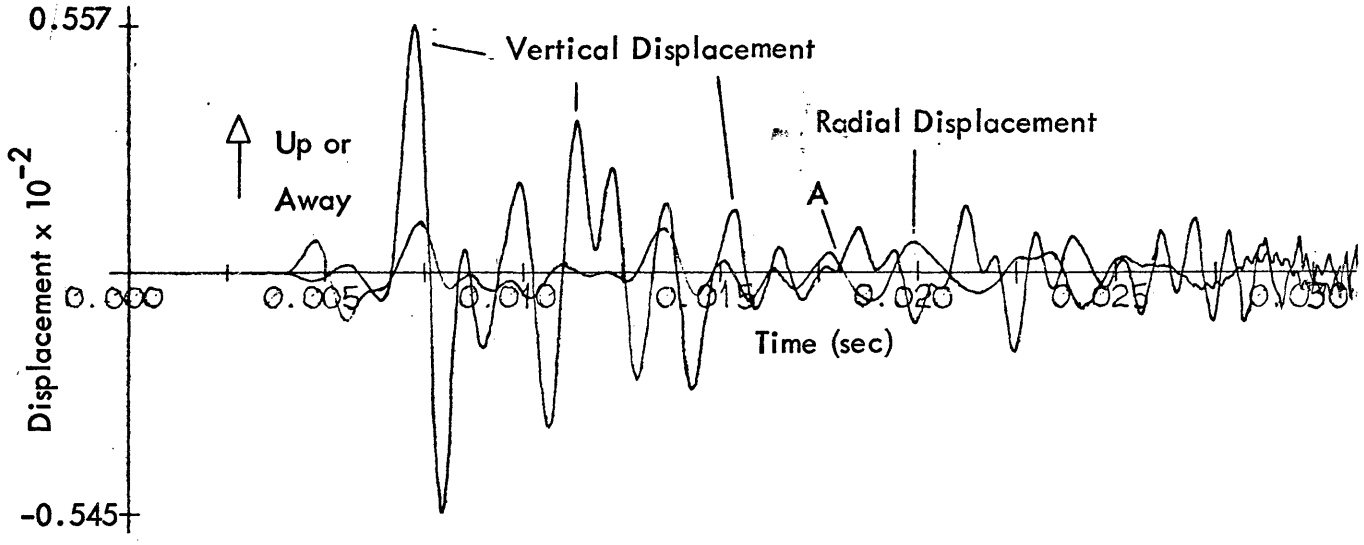

Figure 21a. Displacements 10 m from the axis of symmetry, 0.3 m above the coal seam.

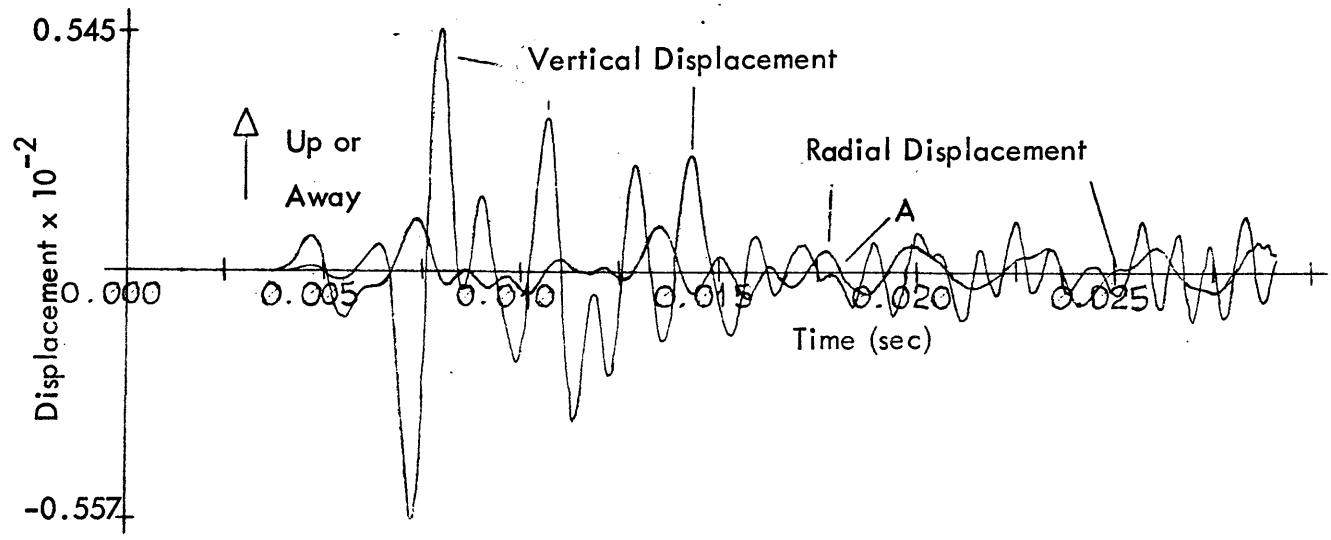

Figure 21b. Displacements 10 m from the axis of symmetry, 0.3 m below the coal seam.

THE CHANNEL WAVE

Recordings of the Channel Wave

Theory presented by Krey(1963) indicates that the phase velocity of any channel wave component lies between the shear velocities of the coal and of the shale. This information places the expected channel wave arrival in a known time window, albeit wide. The most outstanding characteristic of the channel wave should be its amplitude. This is because the channel wave is the manifestation of trapped energy, and the high contrast of acoustic impedances (7 to 1), between the shale and coal, produces favorable conditions for energy entrapment. Positive identification results from the condition that the amplitude of the channel wave should decrease sharply as one moves into the shale, away from the coal seam.

A complete suite of plots of displacements recorded in the coal seam is given in figures 22a through 22g. These plots represent a horizontal string of geophones placed within the coal seam, slightly above the seam's center (1.2 m from the top of the seam, and 1.8 m from the bottom of the seam). The first geophone is at indices (1.6,31.2), which is 1.6 m from the axis of symmetry, on which the source lies. The second is at location (10.0,31.2), or 10 m from the axis of symmetry. The rest of the geophones are at 10 m intervals, except the last, which is at (55.6,31.2), and is near the model's edge, 55.6 m from the axis of symmetry.

The most prominent feature shown in figure 22a is the first break for the radial component (A). As geometry would dictate, the vertical break (B) is smaller. Nothing of import is identifiable here except the first breaks; proximity to the source is responsible for this.

Figure 22b has more character. The first movement at 5 ms (C) is energy critically refracted through the shale; it is very slight. At 7 ms (D) there is

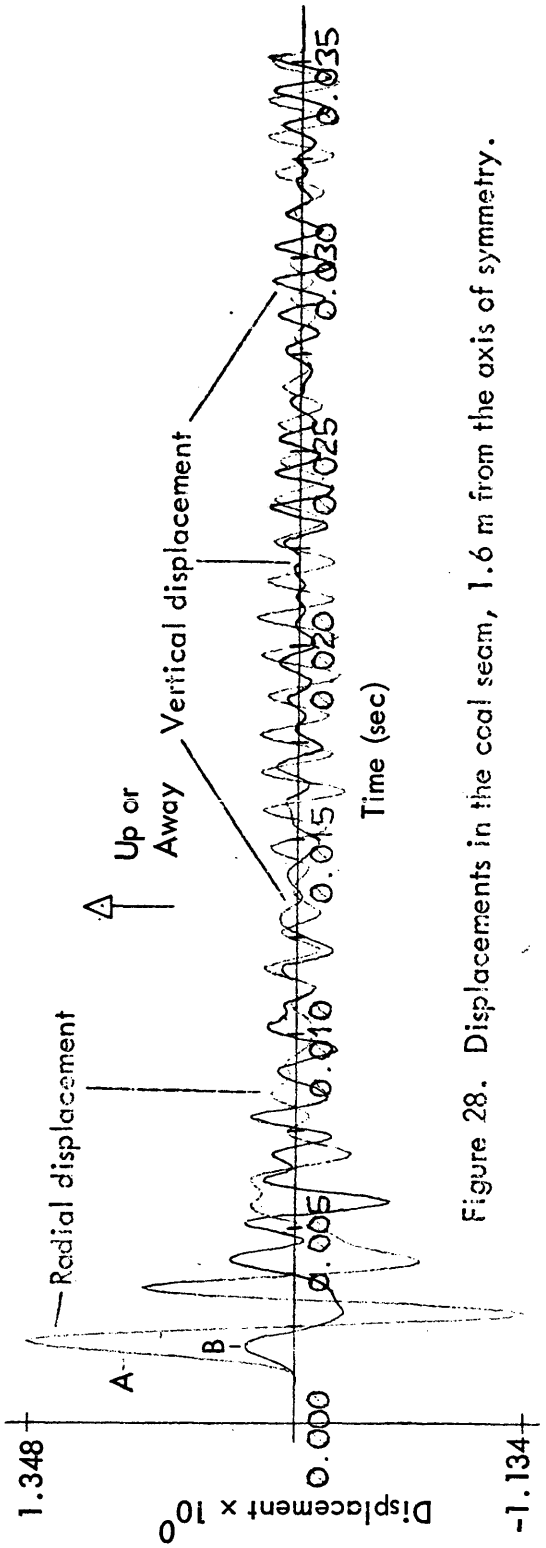

Figure 28. Displacements in the coal seam, 1.6 m from the axis of symmetry.

Figure 22a. Displacements in the coal seam, 1.6 m from the axis of symmetry; depth is 31.2 m.

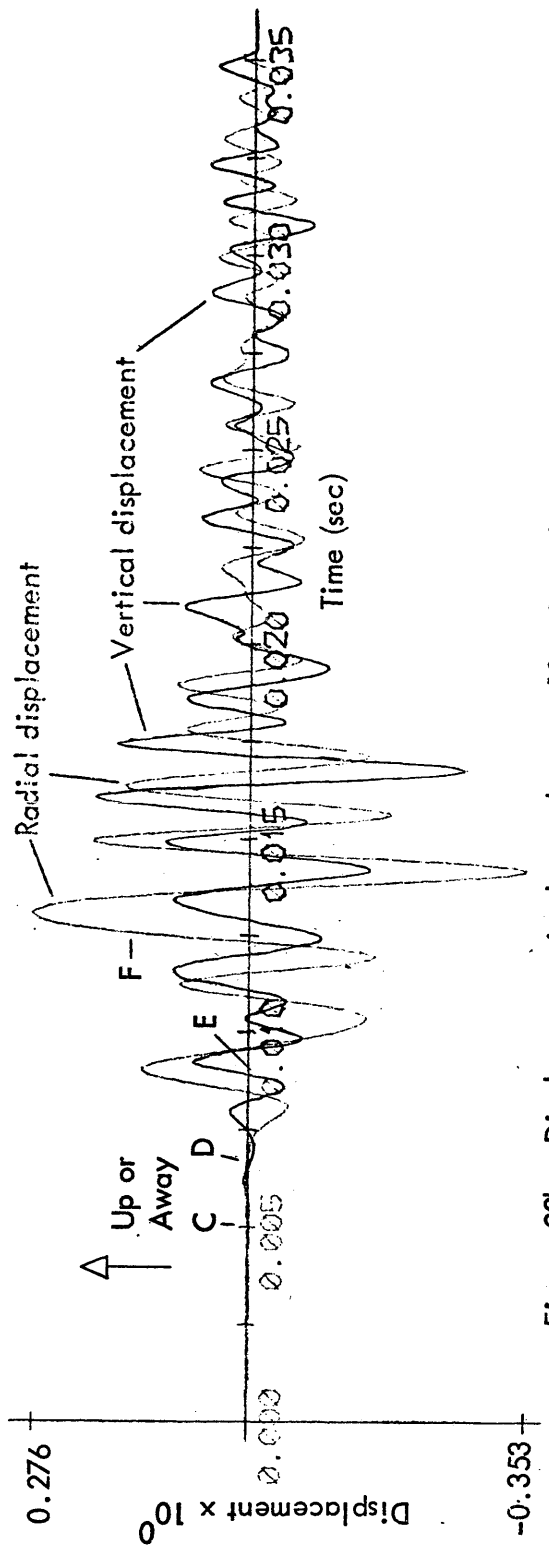

Figure 22b. Displacements in the coal seam, 10 m from the axis of symmetry; depth is 31.2 m.

critically refracted energy from the shear wave in the shale; it is quite noticeable. At 8 ms (E) the direct compressional arrival is apparent. The largest arrival on the record begins at about 12 ms (F). It is radial, and has an amplitude more than double the size of any other radial displacement on the record. Its period is about 2 ms, the same as that of the source.

Figure 22c is perhaps the most interesting of this series of plots. The first arrival (G) is again critically refracted energy travelling as a compressional wave in the shale. The direct compressional wave through the coal should begin at 16.7 ms, and is somewhat buried (H). At 20.5 ms there begins a large radial phase with a period of about 2 ms (I), followed by more phases of comparable amplitude, such as the one with a peak at 25 ms (J). At 29 ms there begins an entire series of high-amplitude, high frequency, nearly monochromatic waves (K), typical of a higher mode Airy phase (in this case it is probably the 2nd higher mode; see figure 32).

Figure 22d gives displacements 30 m from the source. The first distinct phase emerges at 17.5 ms (L). It is shear wave energy in the shale refracting into the coal. At 32.5 ms begins a prominent, radial phase (M), much larger than any of the phases preceding it. Its large amplitude, 2 ms period, and occurence in time lead to the interpretation that this phase correlates to the phase beginning at 20.5 ms (I) in figure 22c, and to the phase beginning at 12 ms (F) in figure 22b. This phase is regarded as the beginning of the channel wave. The reason for the interest in channel wave phenomena is apparent in figures 22b, 22c, and 22d: it dwarfs anything preceding it on the records. Even on a very noisy field record, recorded with simple gear, such a phase would be readily identifiable. The great amount of energy contained in the channel wave will become even more evident when the wave is compared to displacements in the shale around the coal seam. In figure 22c, the high amplitude phases (K) following the first large arrival may also be part of the

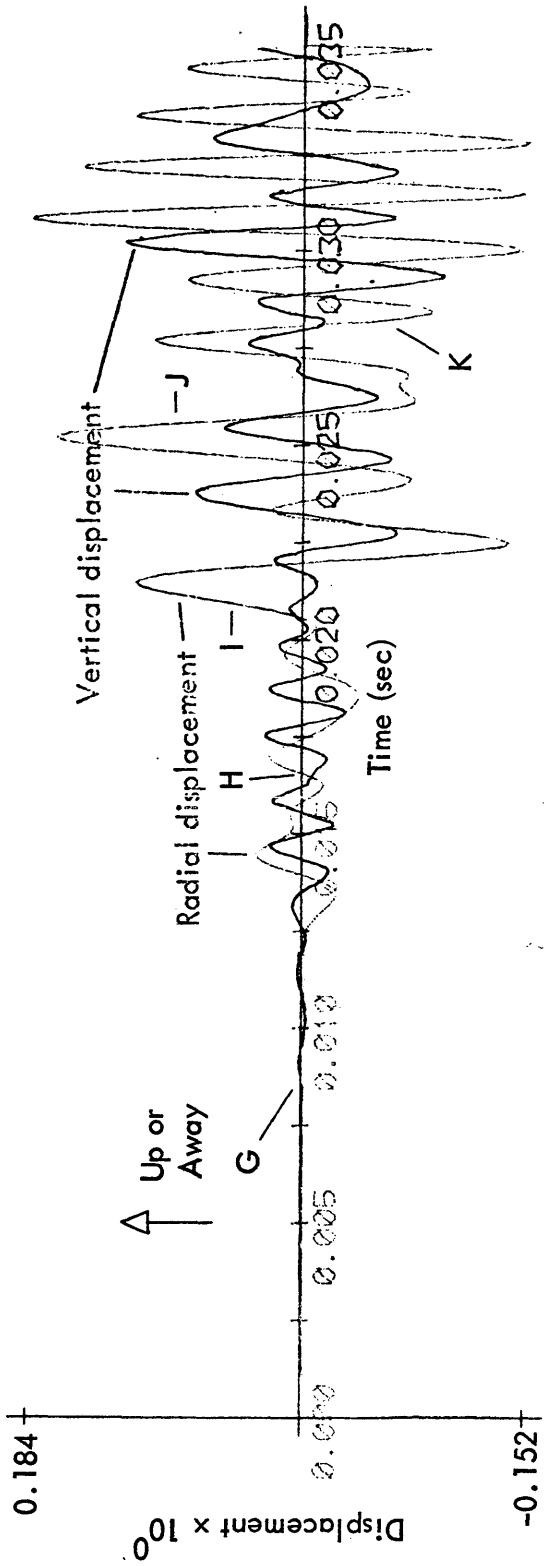

Figure 22c. Displacements in the coal seam, 20 m from the axis of symmetry; depth is 31.2 m.

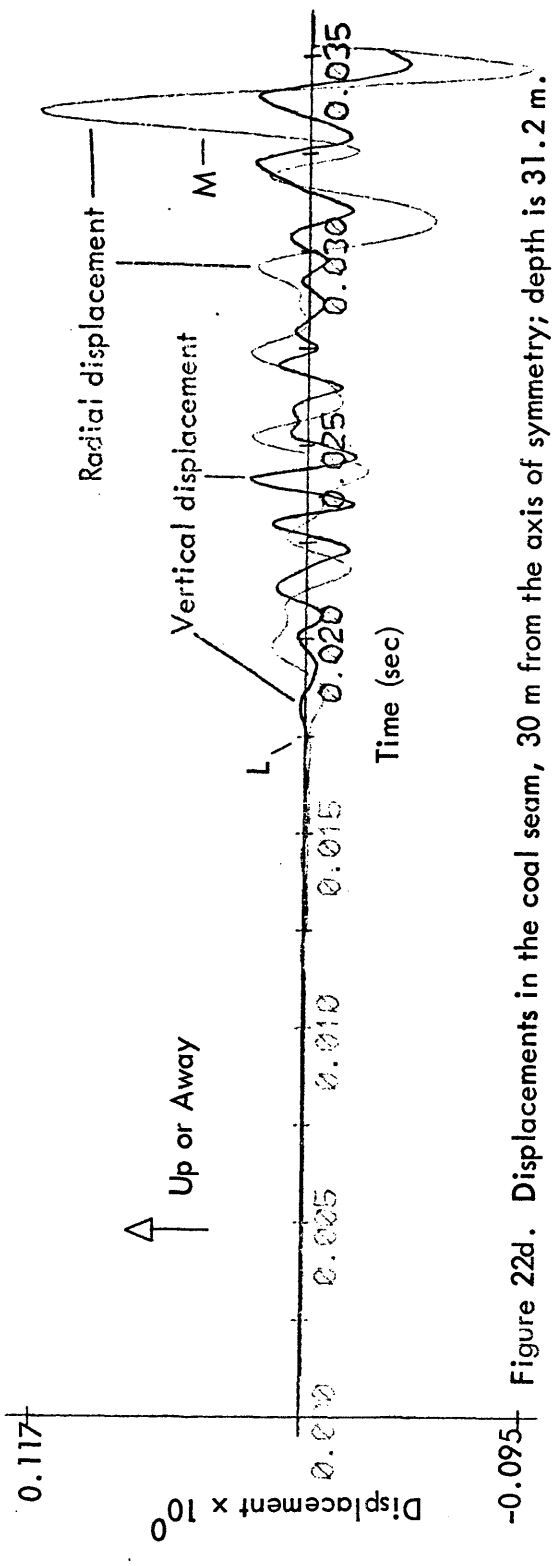

Figure 22d. Displacements in the coal seam, 30 m from the axis of symmetry; depth is 31.2 m.

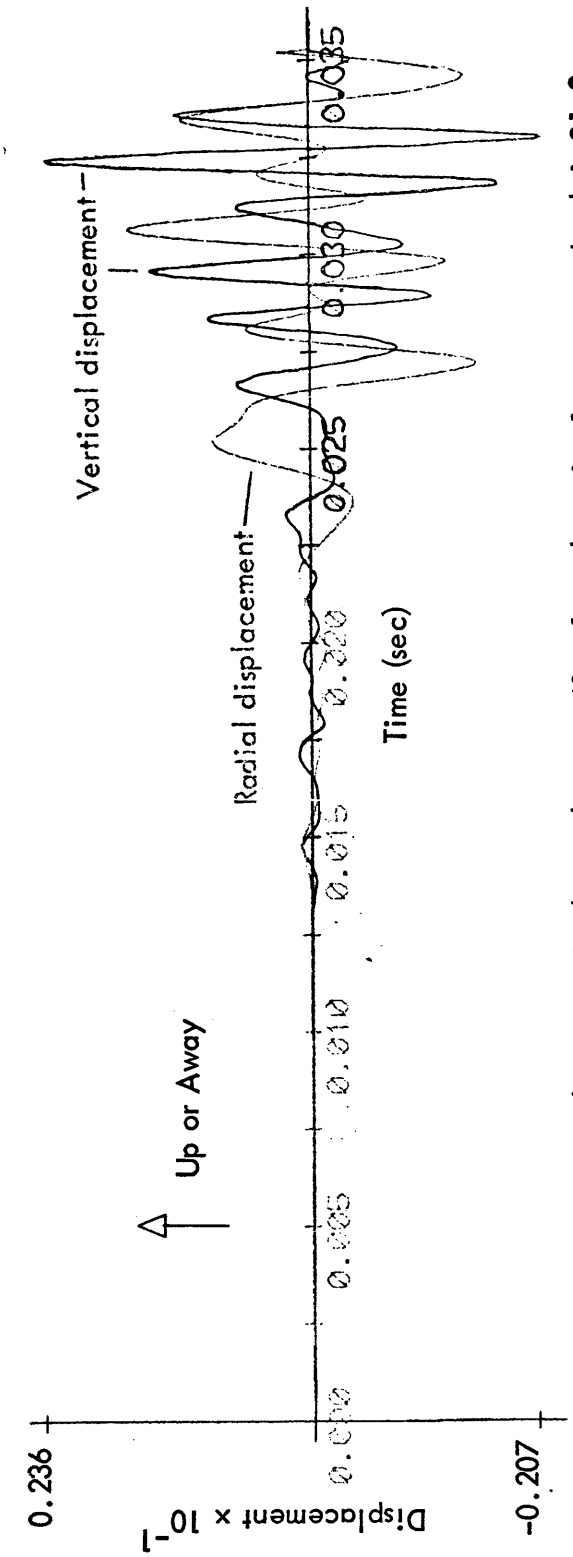

Figure 22e. Displacements in the coal seam, 40 m from the axis of symmetry; depth is 31.2 m.

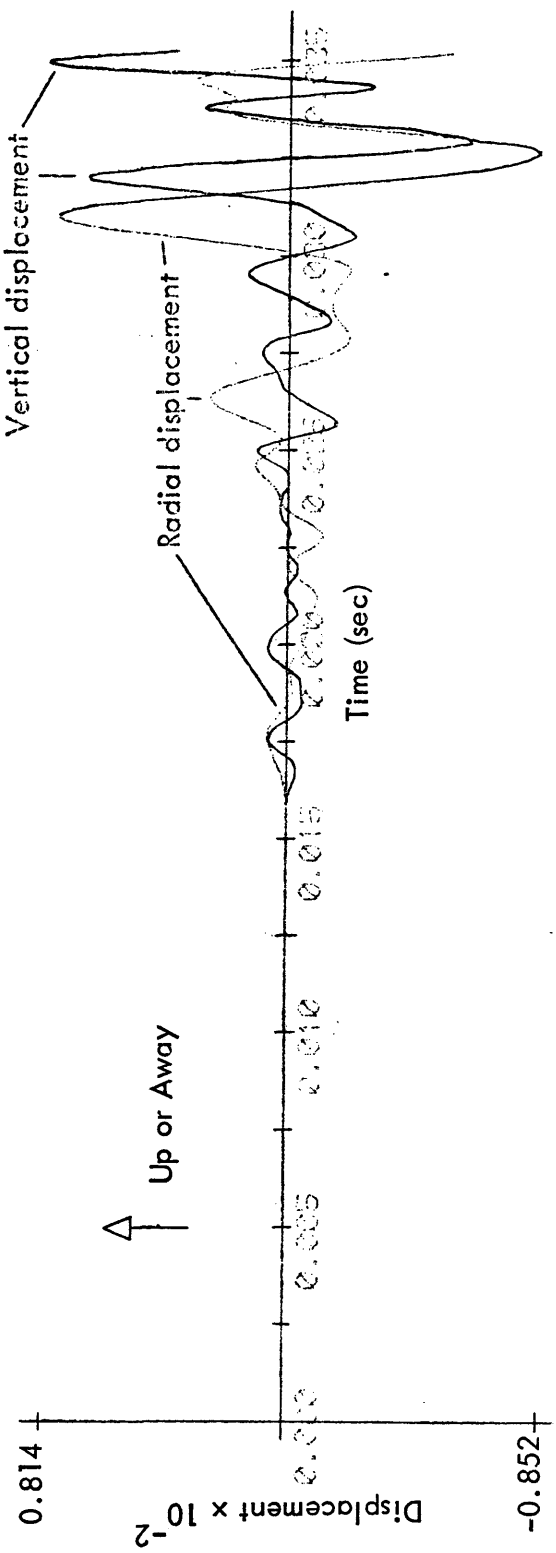

Figure 22f. Displacements in the coal seam, 50 m from the axis of symmetry; depth is 31.2 m.

channel wave train; they are off the record in figure 22d.

Figure 22e is comparable to only the first part of figure 22d, with no channel wave arrival. The reader should note that these plots are all normalized to individual trace maxima and minima, and that these more distant recordings are substantially weaker than the foregoing recordings closer to the source.

Figure 22f and 22g are similar to figure 22e (no channel wave arrival).

There is, then, an anomalously strong event in figures 22b, 22c, and 22d. The radial component is predominant for this phase, and Krey (1963) explains this by assuming that the vertical component of the channel wave is symmetric about the center of the seam; and in fact his measurements support this.

A reorganized presentation of the displacements discussed above is shown in figures 23a and 23b. Figure 23a groups all the radial displacements, and figure 23b groups all the vertical displacements. These figures are in format (2). As each trace is individually normalized, the bottom three traces appear to have surprisingly large amplitudes. This is because the top three traces normalize on the channel wave, which is not present in the lower three. On these plots it is easier to see that the channel wave is just barely caught at location (30.0,31.2), and is not present at all at (40.0,31.2).

Figures 24a and 24b are another presentation of the displacements in the coal seam; they are in format (3). Figure 24a is radial displacement, and figure 24b is vertical. In these figures each trace bears its true amplitude relative to the other traces. The radial traces are deceptively displayed, as they normalize on the large radial break next to the source; the reader should note their absolute amplitude, as indicated by the maxima and minima numbers. In figure 24a it can be observed that the channel wave is the only readily observable disturbance at 20.0 m and 30.0 m from the source (in a radial direction). Its onset is marked by the letter 'A'. The reader may have drawn

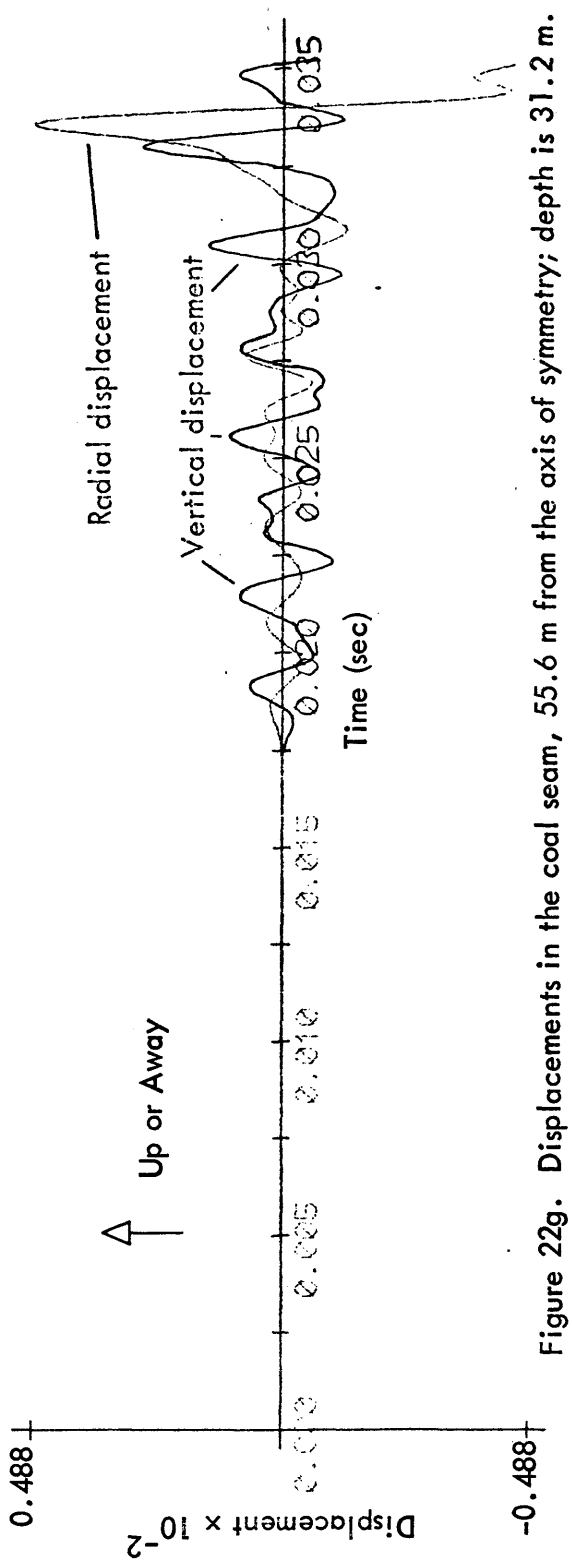

Figure 22g. Displacements in the coal seam, 55.6 m from the axis of symmetry; depth is 31.2 m.

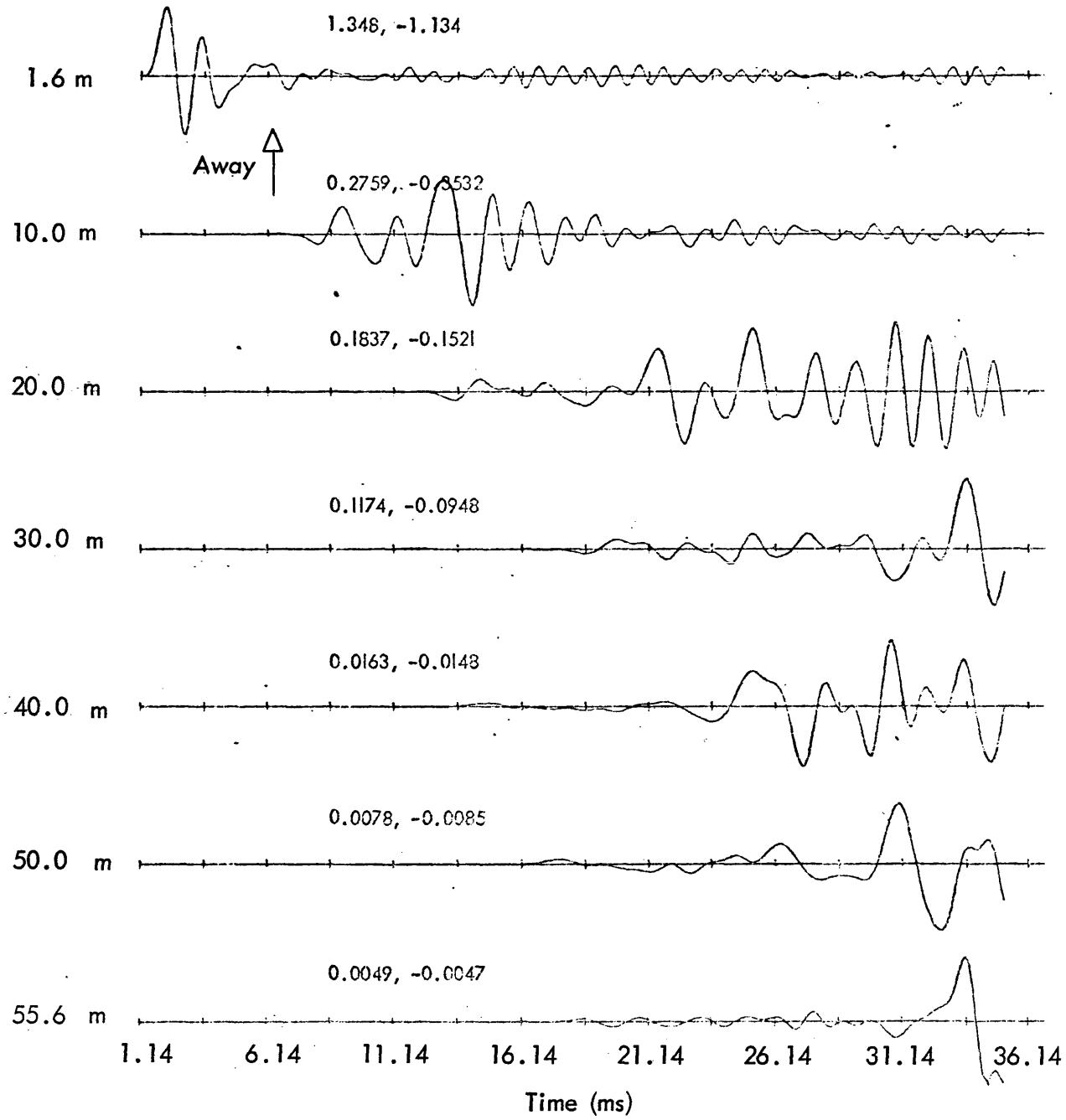

Figure 23a. Radial displacements in the coal seam at a depth of 31.2 m; format (2). Distance from the axis of symmetry is noted to the left of each trace.

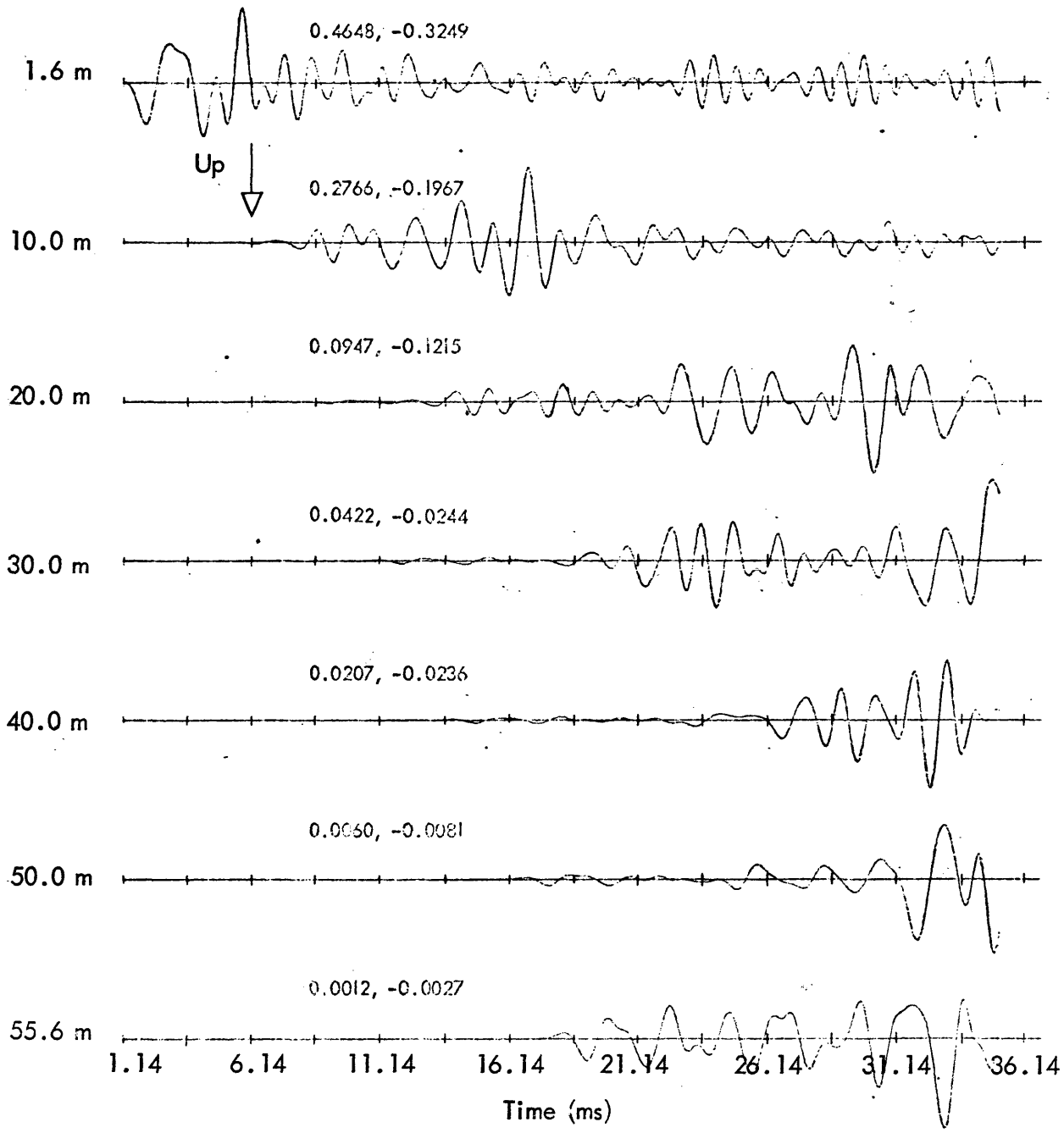

Figure 23b. Vertical displacements in the coal seam at a depth of 31.2 m; format (2). Distance from the axis of symmetry is noted to the left of each trace.

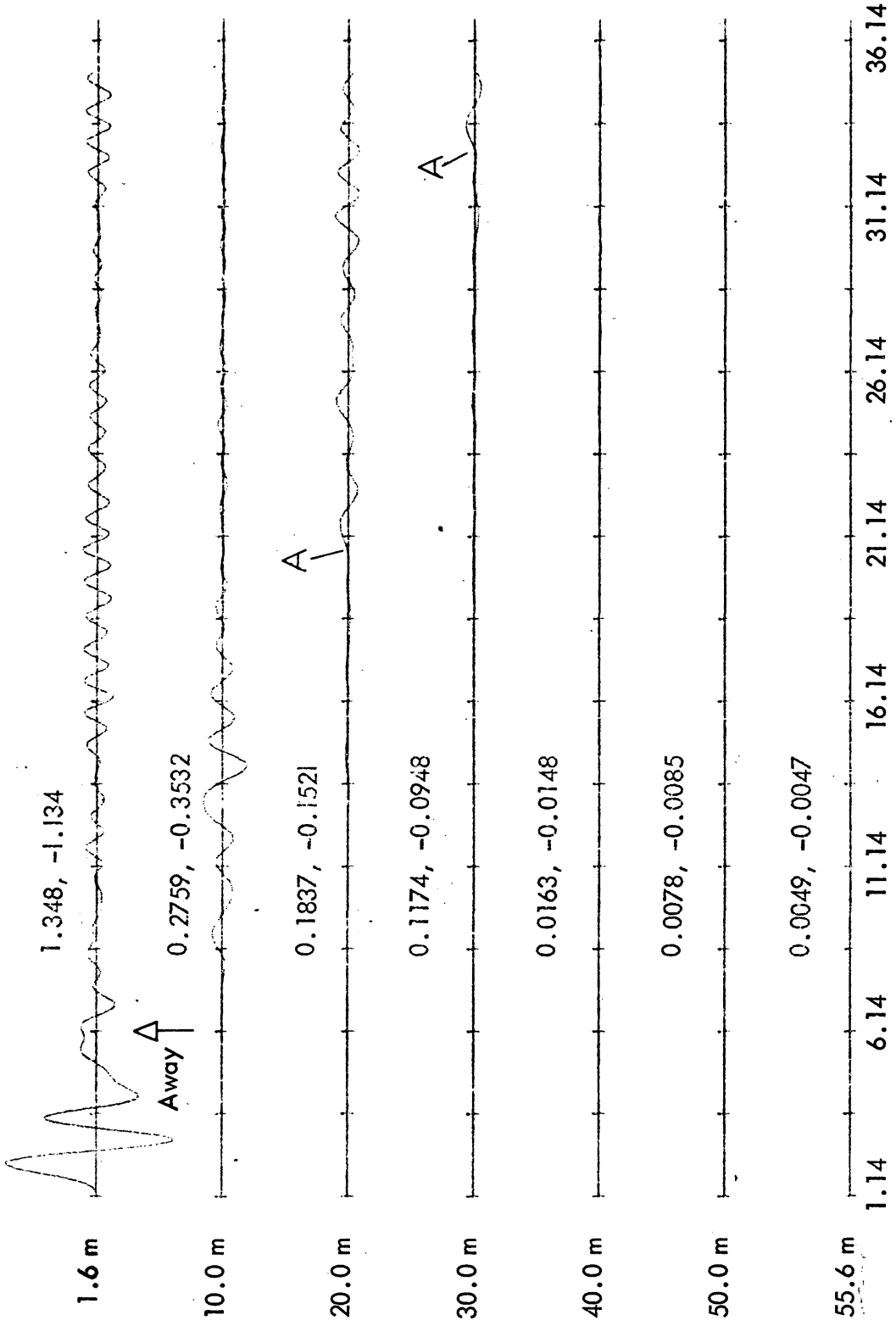

Figure 24a. Radial displacements in the coal seam at a depth of 31.2 m; format (3). Distance from the axis of symmetry is noted to the left of each trace.

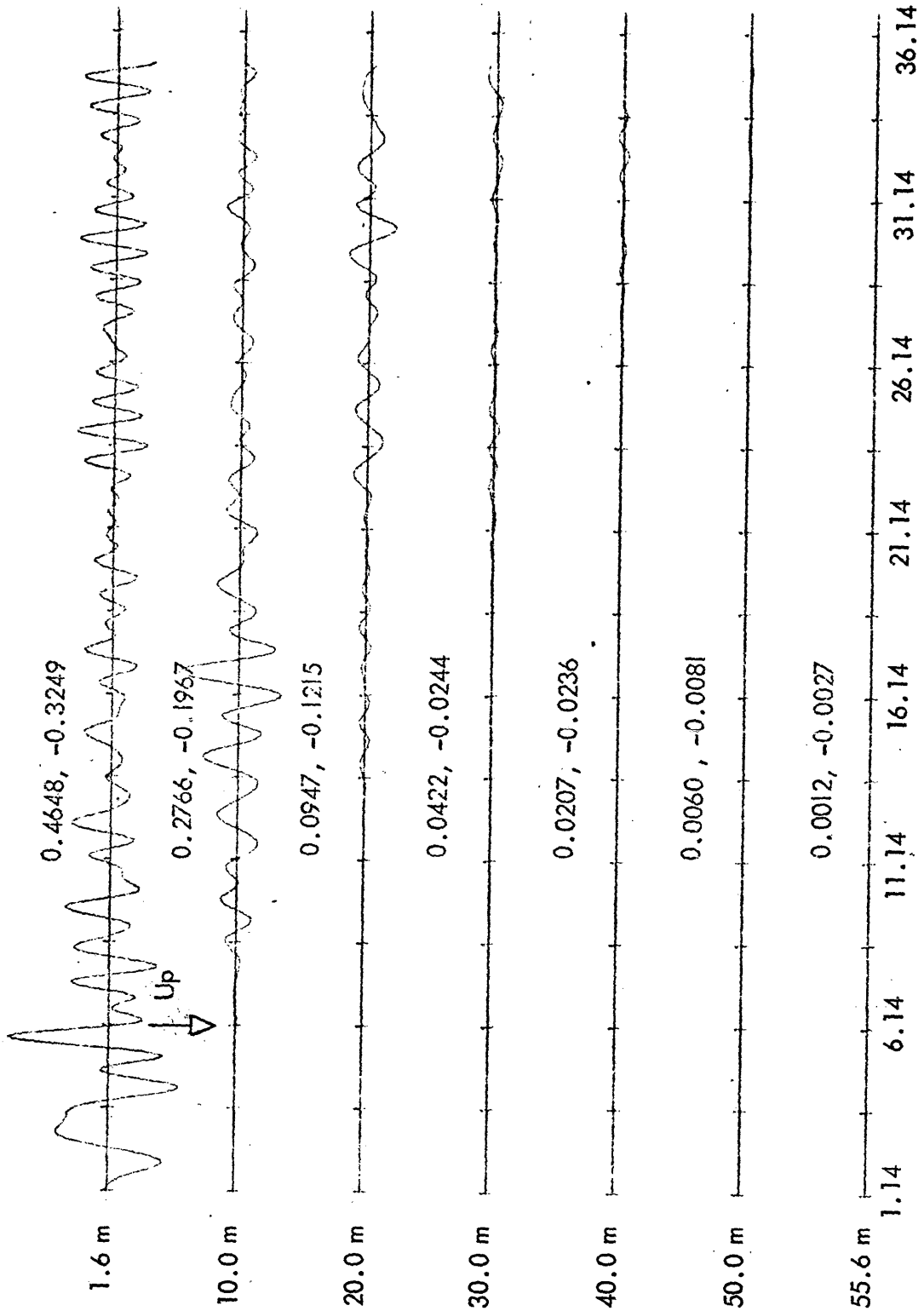

Figure 24b. Vertical displacements in the coal seam at a depth of 31.2 m; format (3). Distance from the axis of symmetry is noted to the left of each trace.

the premature conclusion that the channel wave seems to die out quickly as it moves down the seam. This is illusory, and is discussed below.

The Strength of the Channel Wave

An important question to be answered is in regard to the proportion of energy trapped within the coal seam. As stated previously, a requirement of the channel wave is that it die out quickly in the shale, away from the coal; this will be shown to be true.

Figures 25a and 25b are a clear demonstration that at 20 m from the source the channel wave is overwhelmingly the strongest wave in the medium, and is sharply attenuated as little as 0.3 m above the seam. These figures are in format (3); like the previous figures, each trace maintains a true amplitude relative to the other traces in its group. Now, however, the traces represent a vertical string of geophones at a distance of 20 m from the axis of symmetry. The top trace is at the free surface; the next is in the center of the overlying shale bed; the third, fourth, and fifth traces are in the shale directly above the coal seam; the bottom trace lies within the coal seam, and is the same as that shown in the preceding figures. In figure 25a, which is the radial displacement, it is evident that the channel wave is much stronger than anything in the shale. In fact, the maximum peak-to-peak excursion in the coal exceeds that in the shale immediately above it (at (20.0,29.7)) by a factor of 42, and that of the surface wave by a factor of 18. For the vertical displacement the same factors are, respectively, 3.6 and 13.7 in spite of the fact that the bottom trace was near the center of the seam, which is a null plane for the vertical component.

At a distance of 30 m from the source (grid column 76), the figures in Table 4 may be listed. These numbers indicate a diminished, but still strong contrast, well exceeding an order of magnitude for the radial component. The radial displacements given for the shale are amplified somewhat due to a tuned

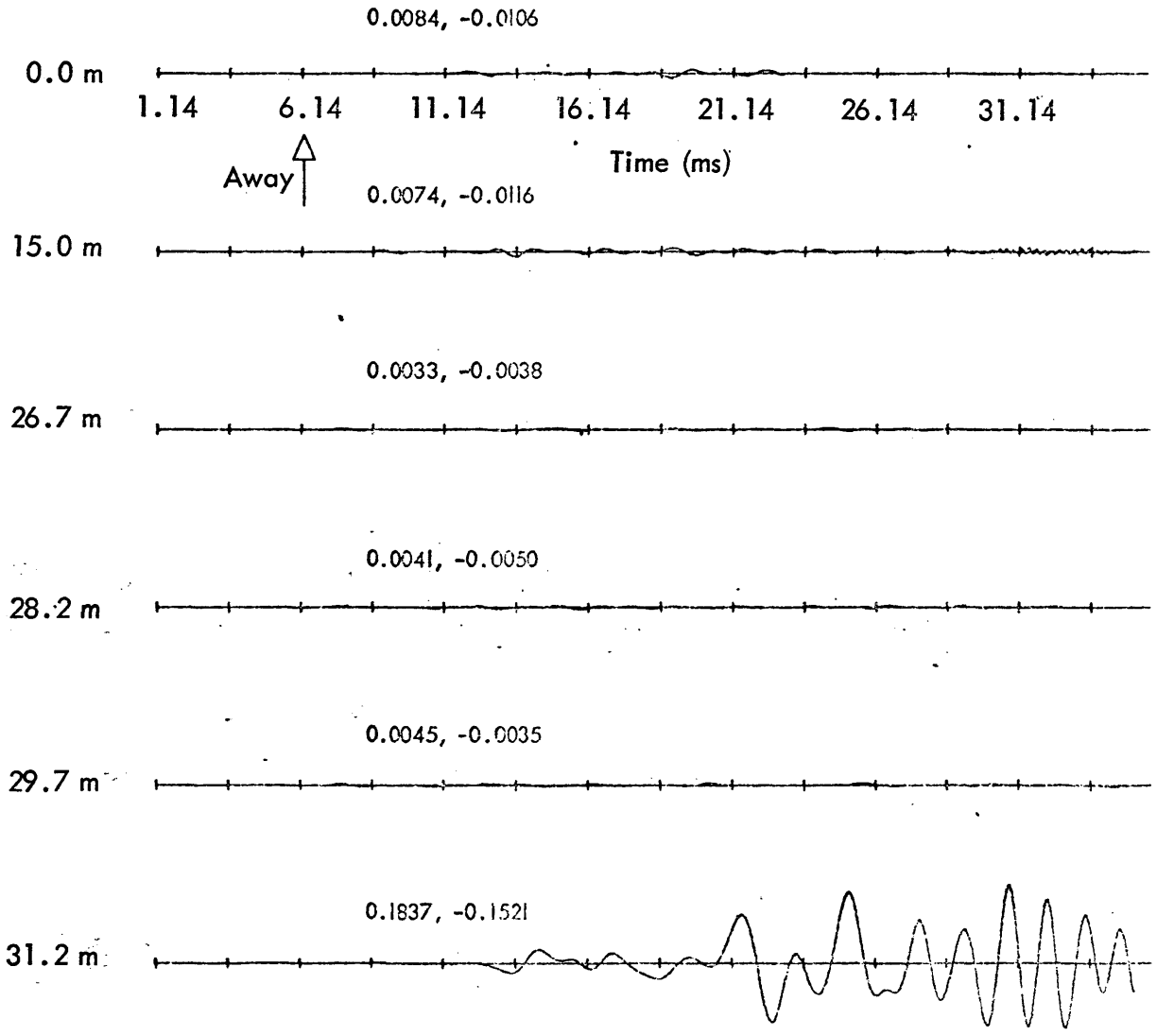

Figure 25a. Radial displacements in a vertical column of geophones 20 m from the axis of symmetry; the bottom trace, at a depth of 31.2 m, is in the coal seam; format (3). Depth from the free surface is noted to the left of each trace.

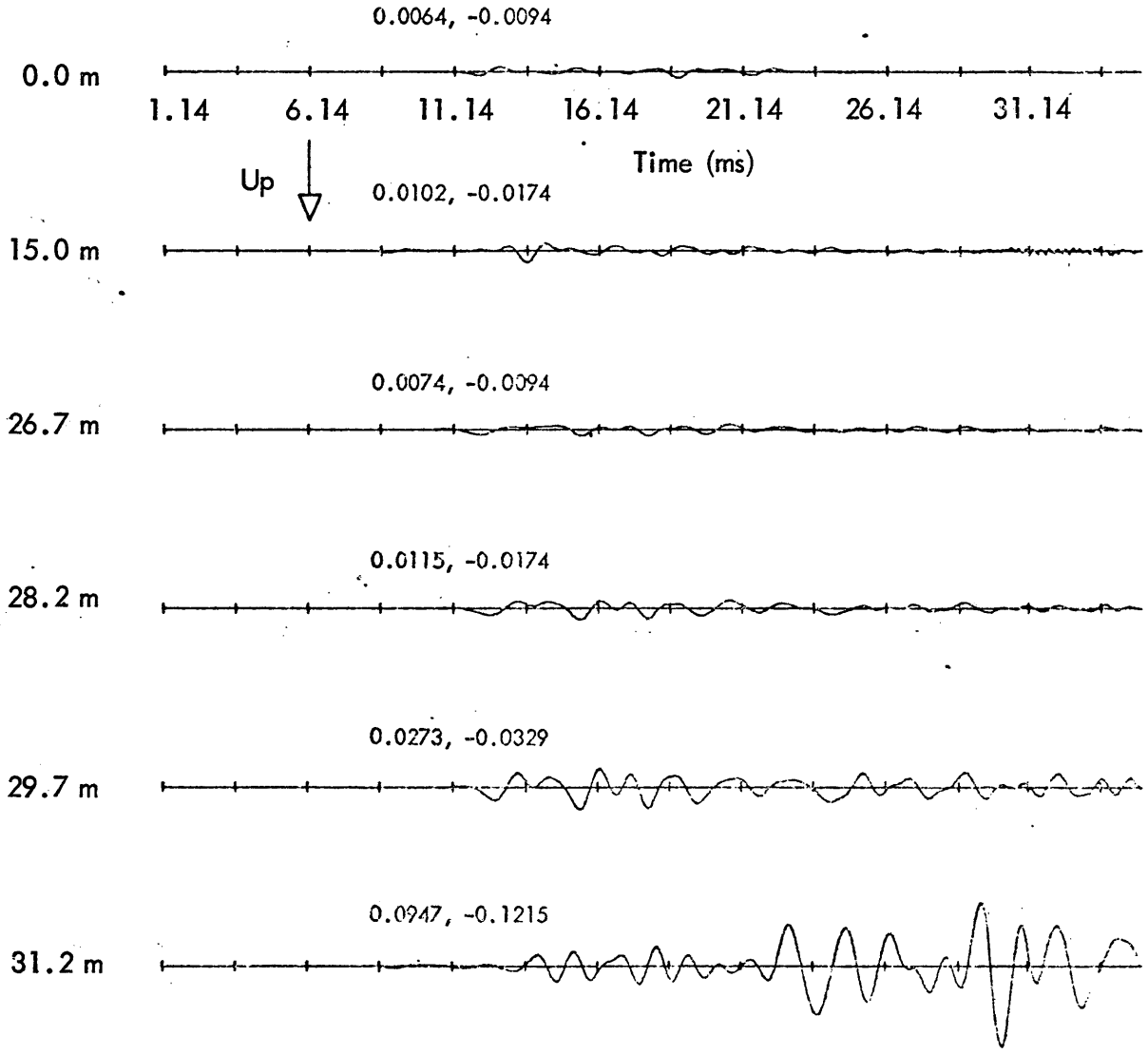

Figure 25b. Vertical displacements in a vertical column of geophones 20 m from the axis of symmetry; the bottom trace, at a depth of 31.2 m, is in the coal seam; format (3). Depth from the free surface is noted to the left of each trace.

Table 4

Maximum and minimum displacements recorded at a column of geophones, 30 m from the axis of symmetry.

Indices	Depth(m)	Lithology	Maximum Radial Displacement	Minimum Radial Displacement	Maximum Vertical Displacement	Minimum Vertical Displacement
(30.0,26.7)	26.7	Shale	0.0045	-0.0042	0.0067	-0.0050
(30.0,28.2)	28.2	Shale	0.0027	-0.0034	0.0122	-0.0083
(30.0,29.7)	29.7	Shale	0.0040	-0.0034	0.0240	-0.0171
(30.0,31.2)	31.2	Coal	0.1174	-0.0948	0.0422	-0.0244

reflection from the outer edge of the model. It is especially evident for (30.0,26.7).

Figures 26a and 26b are in format (3) also, and represent a vertical string of geophones at grid column 101, 40 m from the axis of symmetry. Again, there is one geophone in the coal, at (40.0,31.2). It is notable that even here, where the channel wave, or at least the great bulk of it, has not yet arrived, the main portion of the energy is in the coal seam. This is most evident in the radial displacements shown in figure 26a.

Figures 27a and 27b give a vivid view of the channel wave's entrapment of energy. The plots in these figures are in format (4) - the amplitude of each trace is normalized to a factor proportional to the square root of the distance from the source. Figure 27a gives the radial displacement traces, and figure 27b the vertical displacement traces.

These plots were done to test the idea that the amplitude of the channel wave falls off as the square root of the distance from the source, as would be expected of waves progressing via cylindrical rather than spherical fronts. Normal spherical divergence of energy would require amplitudes to decrease linearly with distance from a point source. As can be seen in figure 27a, cylindrical fronts seem to be appropriate; conclusions are somewhat indefinite because of source proximity and short record length. In any case, there are important observations. It appears that the radial components of displacement at (10.0,31.2) and (20.0,31.2) have comparable power, given the amplitude adjustment. If (10.0,31.2) is full-wave rectified and summed at each time increment from 0 to 20 ms, it adds to approximately 18; 20 ms was chosen as it seems to correspond to the end of an episode which propagates to the end of the trace at (20.0,31 2). If (20.0,31.2) is full-wave rectified and summed for the entire record, it adds to approximately 16. These yield a change-in-amplitude ratio of 9 to 8. If amplitude strictly obeyed a root-of-the-distance-from-the-source law, a ratio of 7 to 5 is expected. If anything, then, the

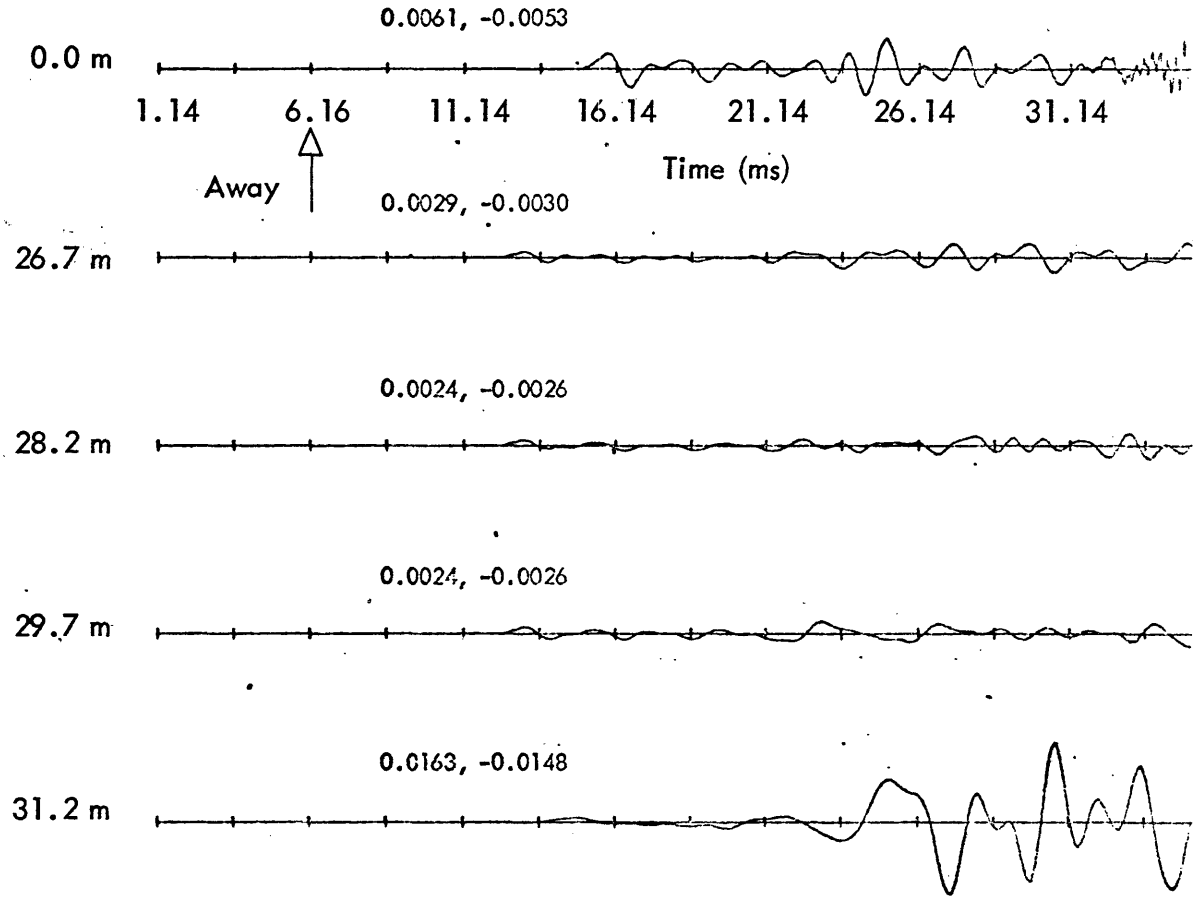

Figure 26a. Radial displacements in a vertical column of geophones 40 m from the axis of symmetry; the bottom trace, at a depth of 31.2 m, is in the coal seam; format (3). Depth from the free surface is noted to the left of each trace.

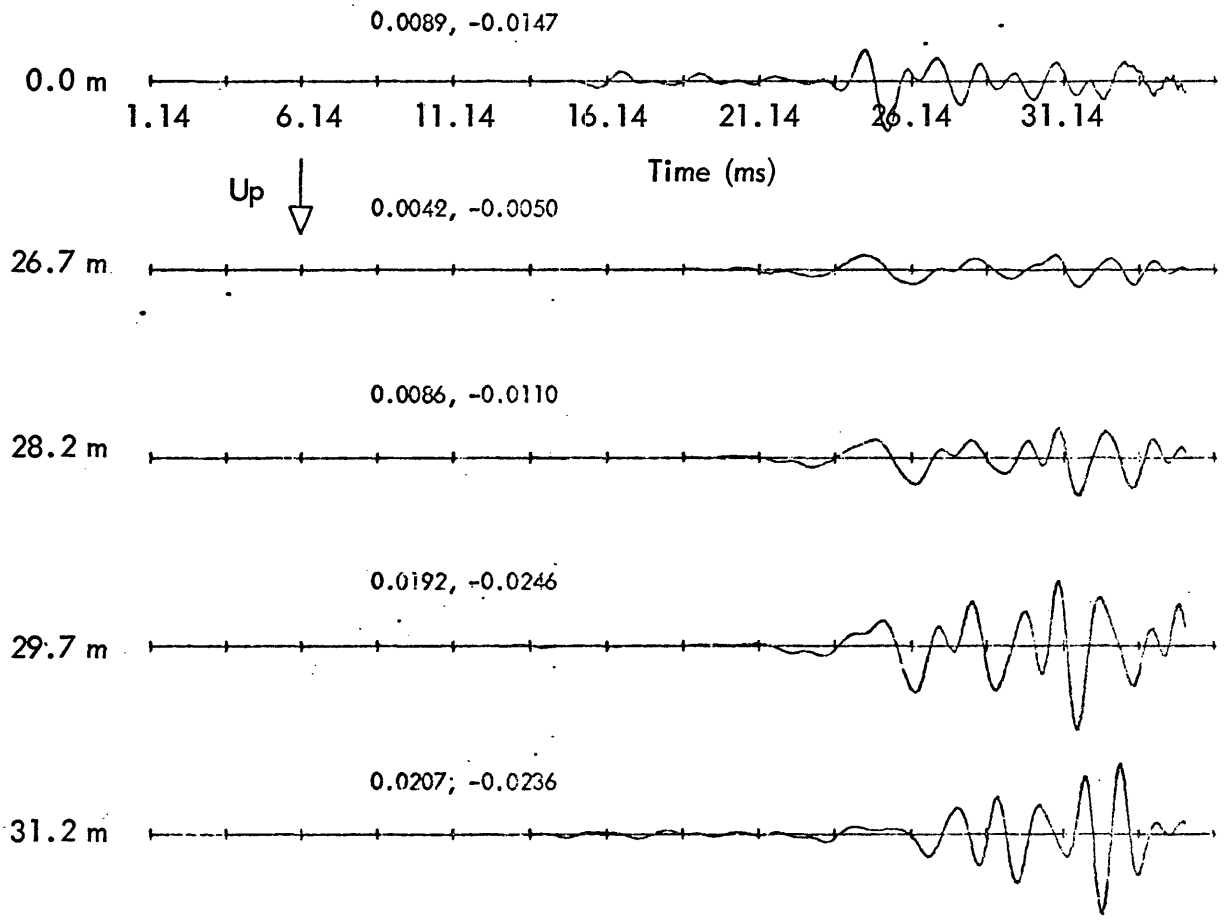

Figure 26b. Vertical displacements in a vertical column of geophones 40 m from the axis of symmetry; the bottom trace, at a depth of 31.2 m, is in the coal seam; format (3). Depth from the free surface is noted to the left of each trace.

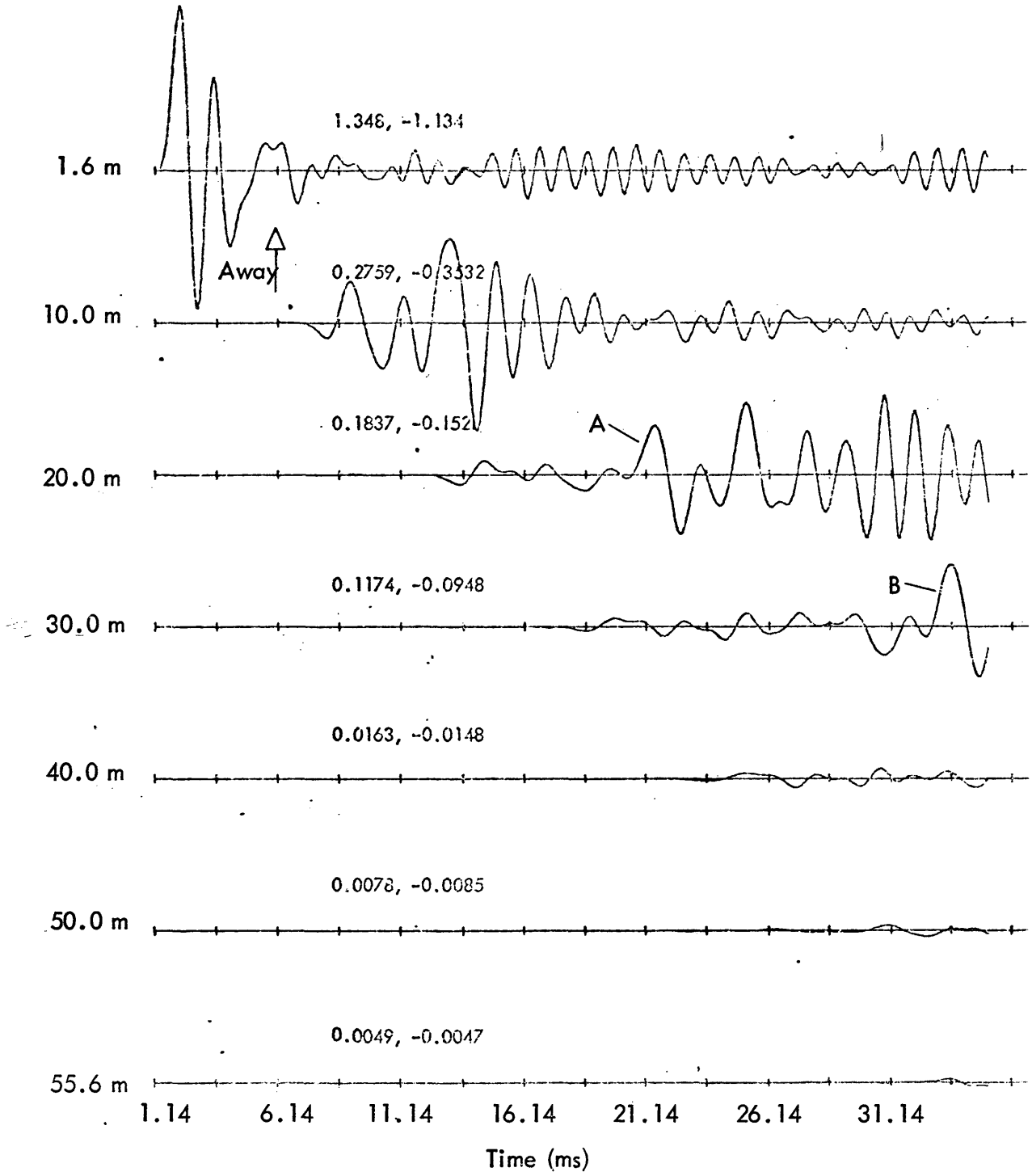

Figure 27a. Radial displacements in the coal seam, with normalization proportional to the square root of the distance from the source; depth is 31.2 m; format (4). Distance from the axis of symmetry is noted to the left of each trace.

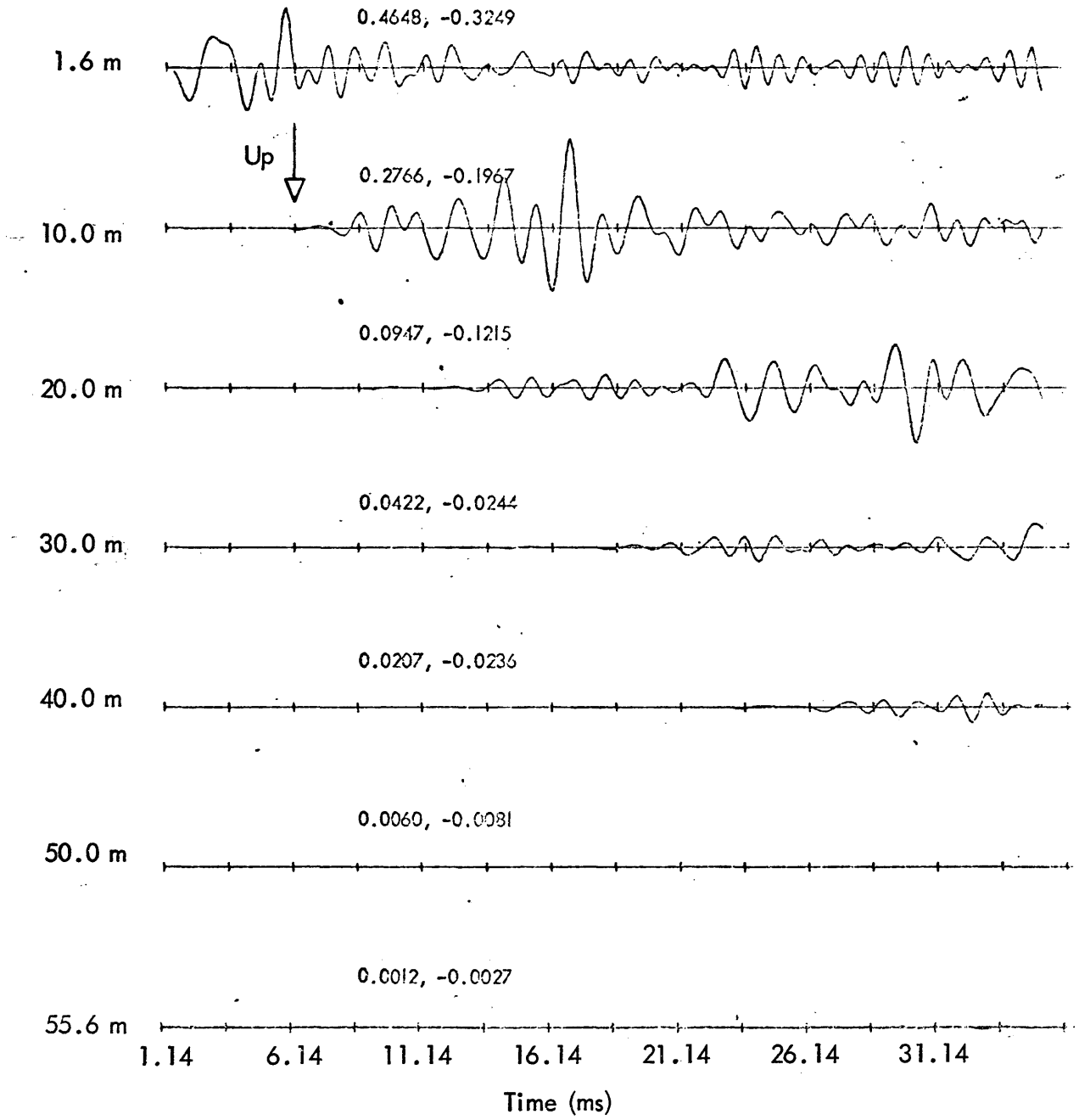

Figure 27b. Vertical displacements in the coal seam, with normalization proportional to the square root of the distance from the source; depth is 31.2 m; format (4). Distance from the axis of symmetry is noted to the left of each trace.

9 to 8 ratio is very encouraging, as at this distance it would indicate that energy is being lost at less than a linear rate. At (30.0,31.2) only the first large pulse (B) of the channel wave is recorded, but in figure 27a it can be seen that after normalization this pulse has the same peak-to-peak amplitude as the corresponding arrival at (20.0,31.2) (A). This is positive evidence that amplitude falls off only as the square root of the distance from the source.

Ray Analysis of Channel Waves

One way to explain the channel wave phenomenon is to regard it as a collection of many body-wave rays. In a thin seam such as the one modeled here, there would, in short order, be a large number of rays bouncing back and forth in the seam with numerous mode conversions. An elementary example of this is given in figure 28. The geophone whose output is plotted lies on the axis of symmetry, and is in the shale 3.3 m above the top of the coal seam. Between 20 and 25 ms the beginning of the instability can be observed. Preceding the instability the trace exhibits a strong periodicity of 2.5 ms. It happens that it takes the compressional wave in coal exactly 2.5 ms to travel the vertical dimension of the coal seam; this implies that the periodic character observed is simply a series of 'multiples' from within the seam. This sort of reflection takes place along the entire length of the coal seam, and the superposition of these reflections assumes a diverse, complex character, whose expression is the channel wave.

An investigation of this ray theory concept was done with the aid of a computer program written by C. H. Yang of the Colorado School of Mines (1974). This program computes the arrival time of a ray at any geophone location. As used in the program, a ray is described as follows: let the model be composed of three layers, layer 1 being 30 m of shale, layer 2 being 3 m of coal, and layer 3 being 30 m of shale; let P represent a compressional wave,

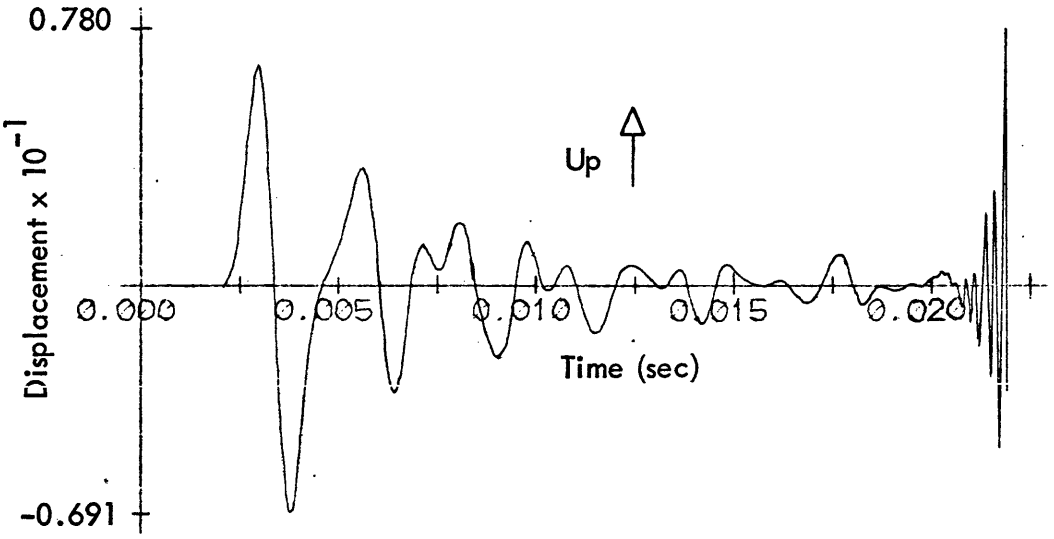

Figure 28. Vertical displacements on the axis of symmetry, 3.3 m above the coal seam.

and S a shear wave; let, for example, a compressional ray-leg in layer 2 be described as P2, and a shear ray-leg in layer 1 as S1; then, a ray which originates at the source in layer 2 as a compressional wave, converts to a shear wave upon transmission to layer 1, and travels to some point in layer 1, would be described as P2S1. The representation of each ray-leg in a ray name (e.g., P1 in P2P1P1) will be called a syllable. Since the source is in the seam and is purely compressional, the first syllable of any ray name must be P2 Yang's program was used to compute arrival times at locations (20.0,31.2) and (30.0,31.2) in the coal seam for all permutations of all rays up to and including five syllables, with the first syllable held to be P2, and all syllables held to be in the coal seam.

Figure 29 indicates the arrival times of these rays at geophone location (20.0,31 2). Several observations can be made. Significant energy, refracted from the shale, arrives before the first compressional arrival through the coal. Rays made up only of P2 syllables definitely do not account for very much of the energy in the channel wave. The channel wave gathers most of its strength after rays of four and five syllables arrive. There seems to be a very significant conversion of energy from the compressional to the shear mode. The primary first arrival for the channel wave appears to be the P2S2P2 ray.

Figure 30 indicates arrival times for the same group of rays at location (30.0,31.2). Comments made for (20.0,31.2) apply, except that the first large pulse of the channel wave is not at the P2S2P2 arrival, but at the arrival of three coincident rays, P2S2S2P2P2, P2S2P2S2P2, and P2P2S2S2P2.

The head waves for the rays discussed above have their first arrivals at (20.0,31.2) marked in figure 31. These arrivals are calculated assuming critical refraction at the coal-shale interface, and the compressional velocity of the shale as the speed in the shale. They precede the purely reflected arrivals by 7 to 9 ms, and do not seem to contribute much of the energy in the channel wave. Their arrival times also imply that (20.0,31.2) is not near

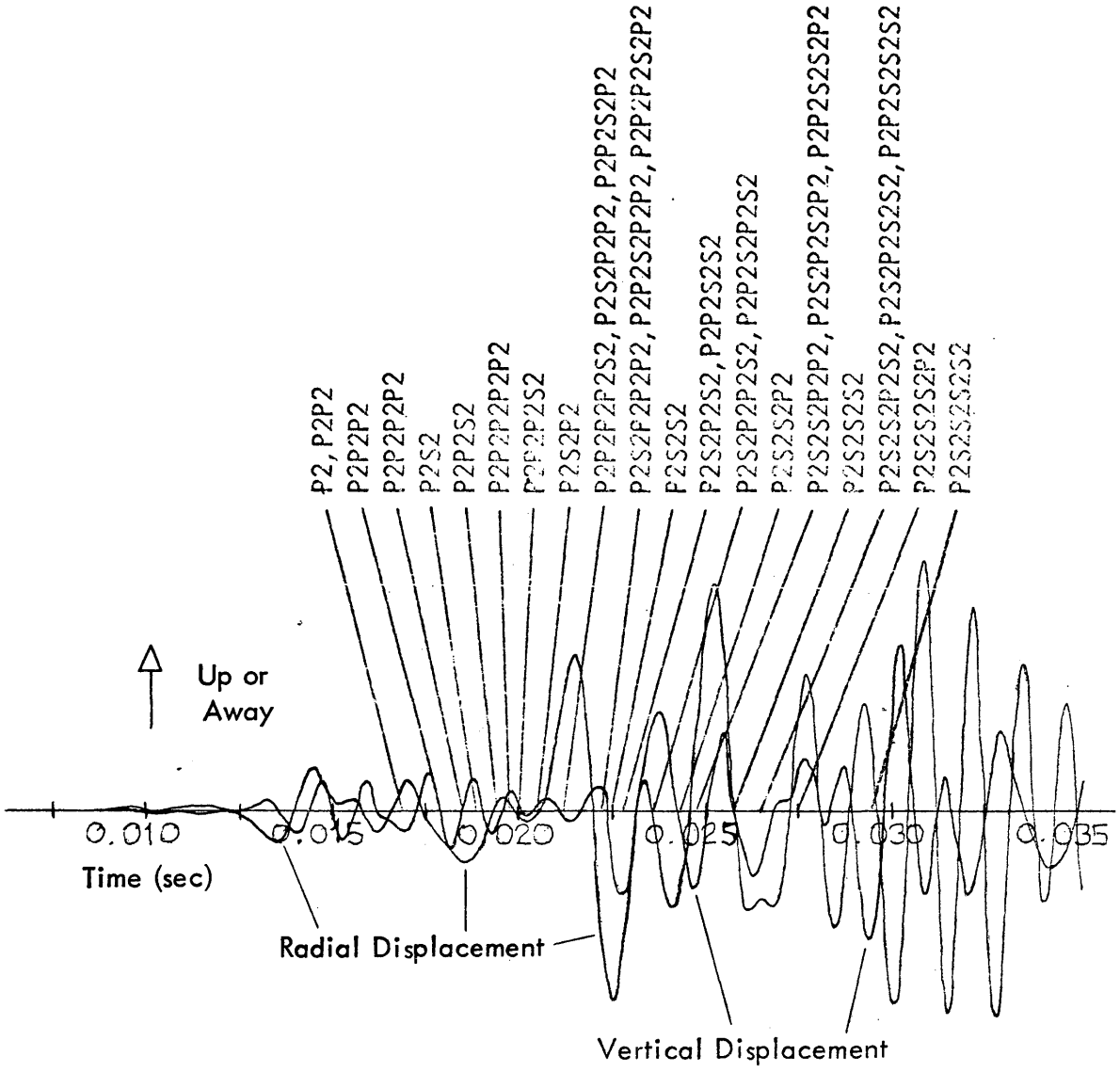

Figure 29. The arrival of rays at a geophone location in the coal seam, at a depth of 31.2 m, 20 m from the axis of symmetry.

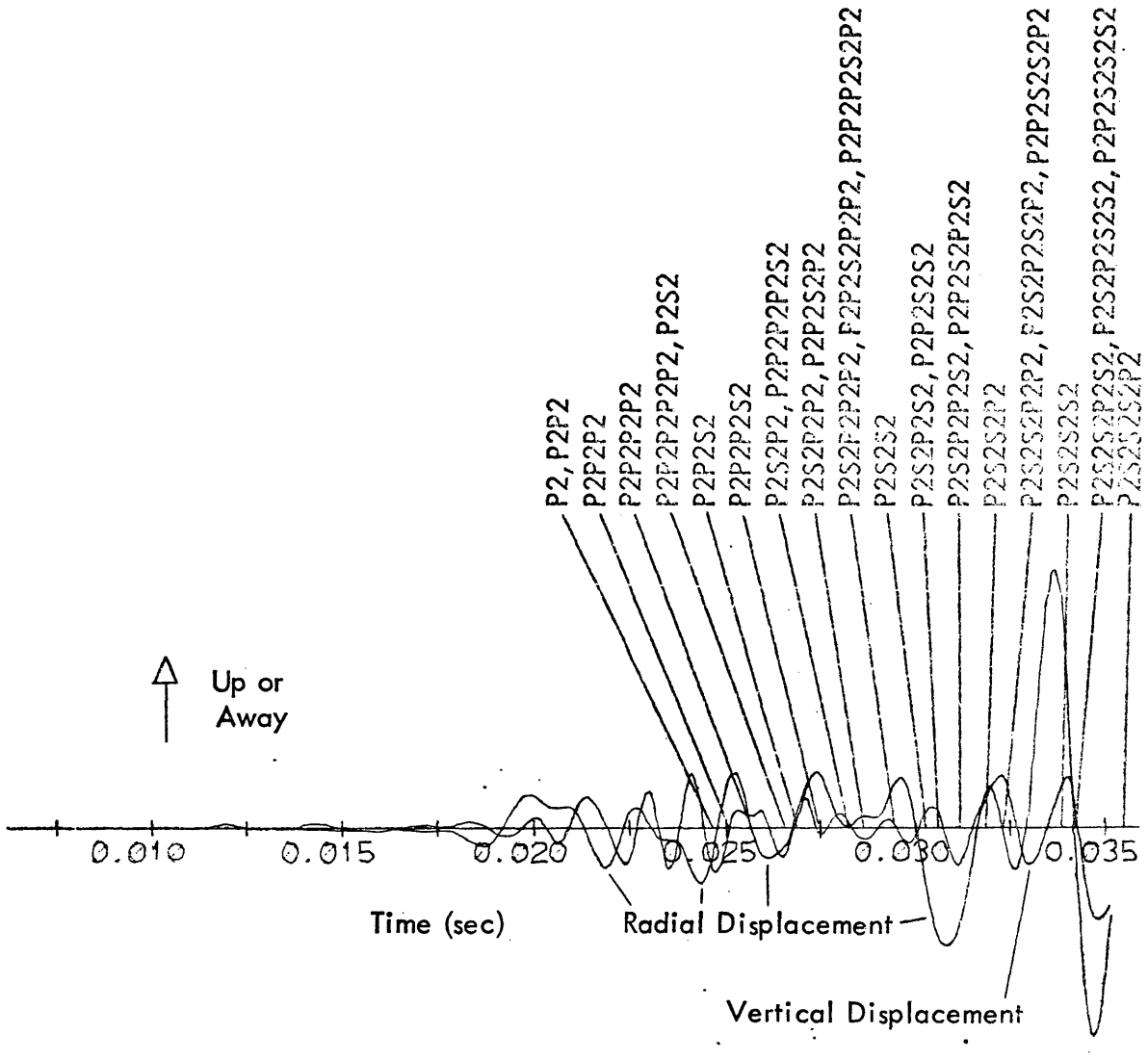

Figure 30. The arrival of rays at a geophone location in the coal seam, at a depth of 31.2 m, 30 m from the axis of symmetry.

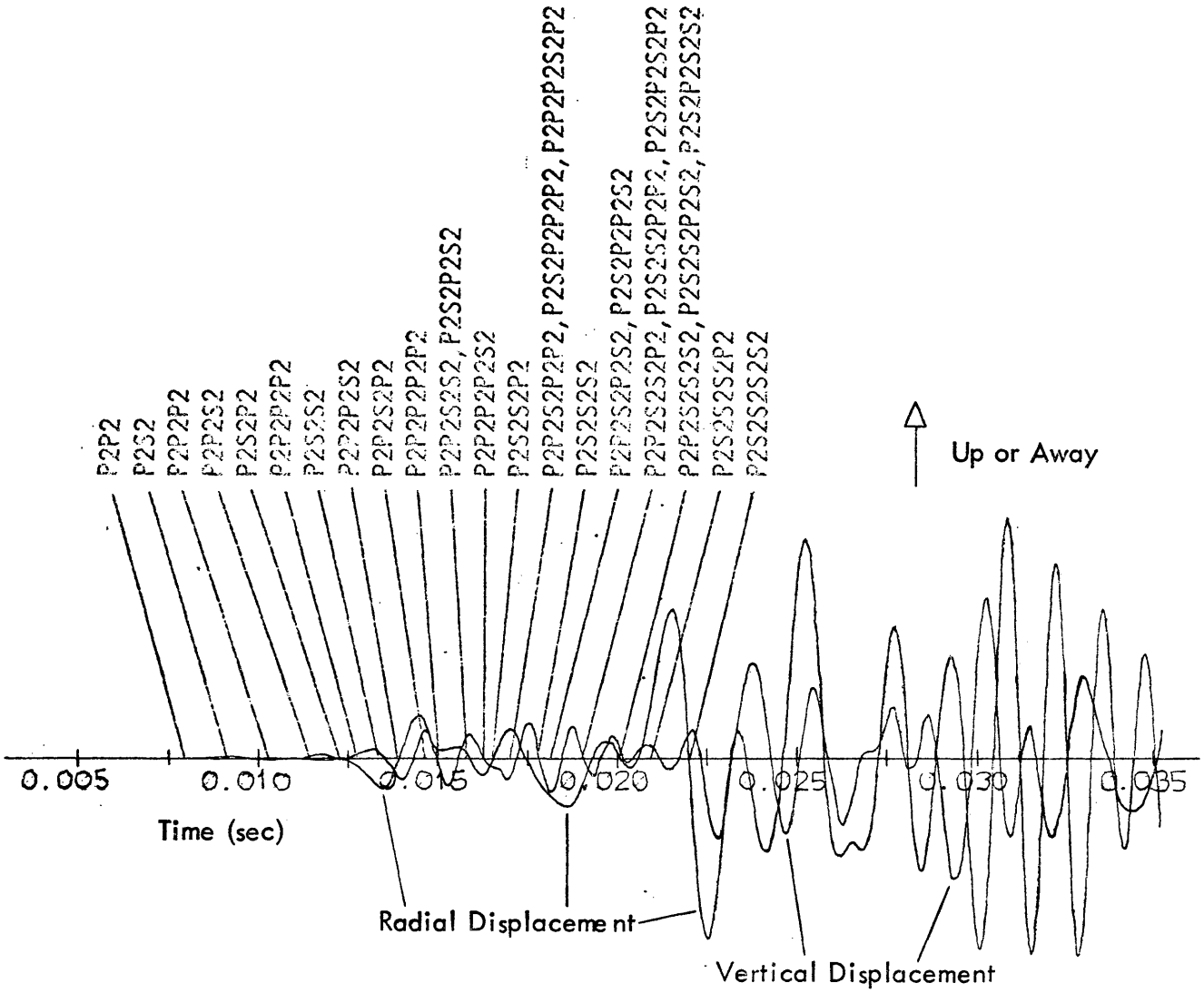

Figure 31. The arrival of the first head-wave rays at a geophone location in the coal seam, at a depth of 31.2 m, 20 m from the axis of symmetry.

a critical distance for any of the rays, as they precede the direct ray arrivals by a considerable margin.

Another suite of critical refractions would be those characterized by shear wave propagation in the shale. Mr. Yang will include these in his PhD thesis, along with appropriate amplitudes.

It is difficult to make any generalization concerning which rays are most responsible for the channel wave. It is reasonable that the rays should vary in importance as one moves down the seam, since the angles of incidence of the legs of the ray would change, and this would affect the energy distribution among the rays.

This exercise well illustrates the nemesis of ray theory. The rays become too numerous for accounting purposes.

Mode Analysis of Channel Waves

Another way of describing the channel wave is in terms of modes. This is the way used by Krey (1963). Reproduced from Krey in figure 32 are the phase and group velocity curves for the first two modes, with the axis scaled to this model. Superimposed are the shear velocity for the shale (v_s), the shear velocity for the coal (v_s'), and a dashed curve representing a relative amplitude spectrum for the source pulse as measured 1.2 m from the point source (see figures 14a,b for a time domain representation). Wavelengths were assigned to the spectrum using the compressional speed of the coal (1200 m/sec), since the source was a compressional source. The transform indicates a strong excitation at a wavelength of 2.2 m, or an approximate period of 2 ms. This plot can be used to compare the model output with Krey's theory.

Figure 33 is a reproduction of the output at (20.0,31.2). Superimposed on it is a trace from figure 8 in Krey (1963). This trace was recorded in a coal seam 2 m thick, at a distance of 21 m from the source, in a radial

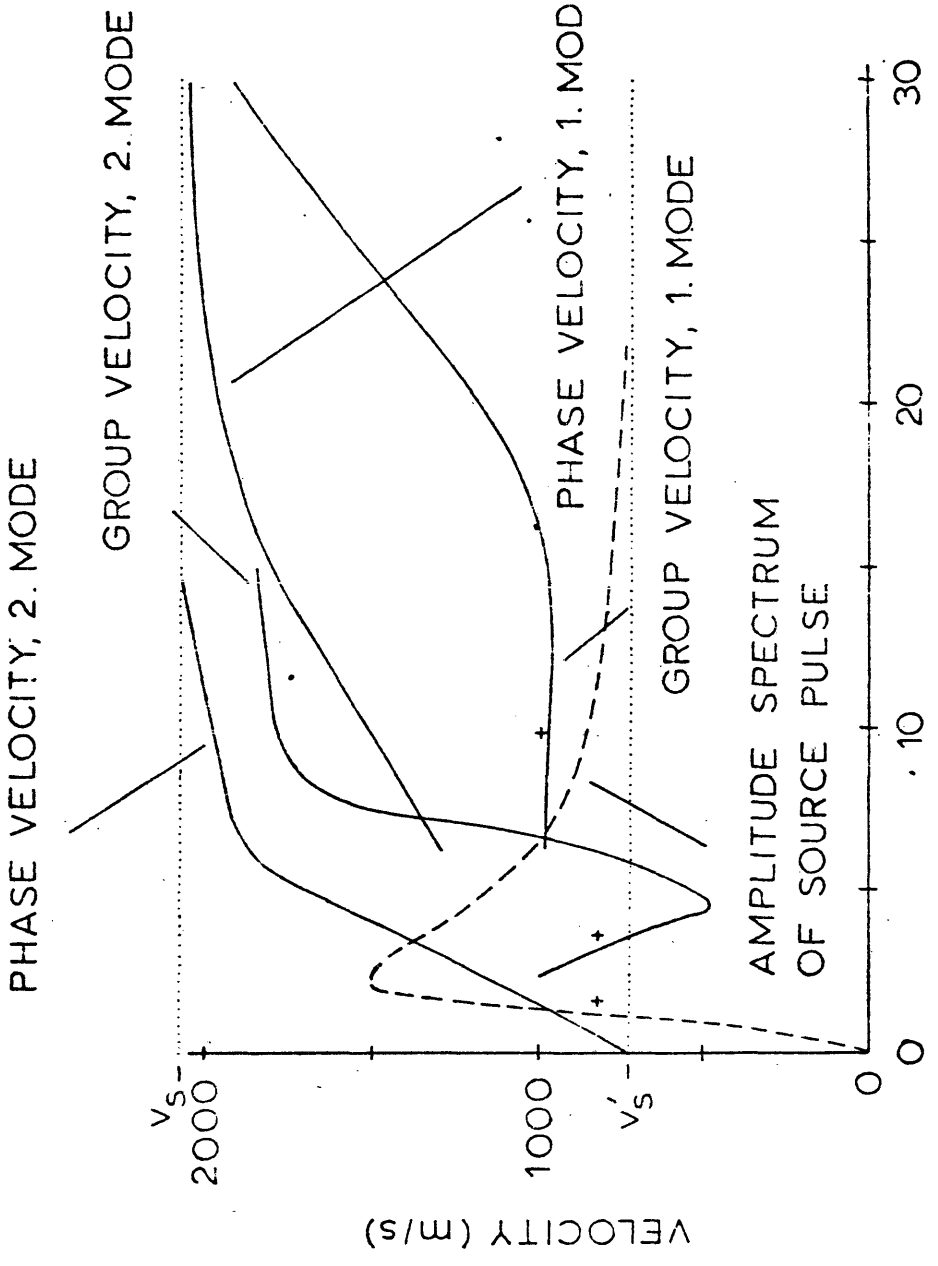

Figure 32. Phase and group dispersion curves for the first and second modes of the channel wave, as adapted from Krey (1963). The dashed line represents the amplitude spectrum of the source pulse, with a relative scale. The shear velocities of the shale and coal are represented, respectively, by v_s and v'_s.

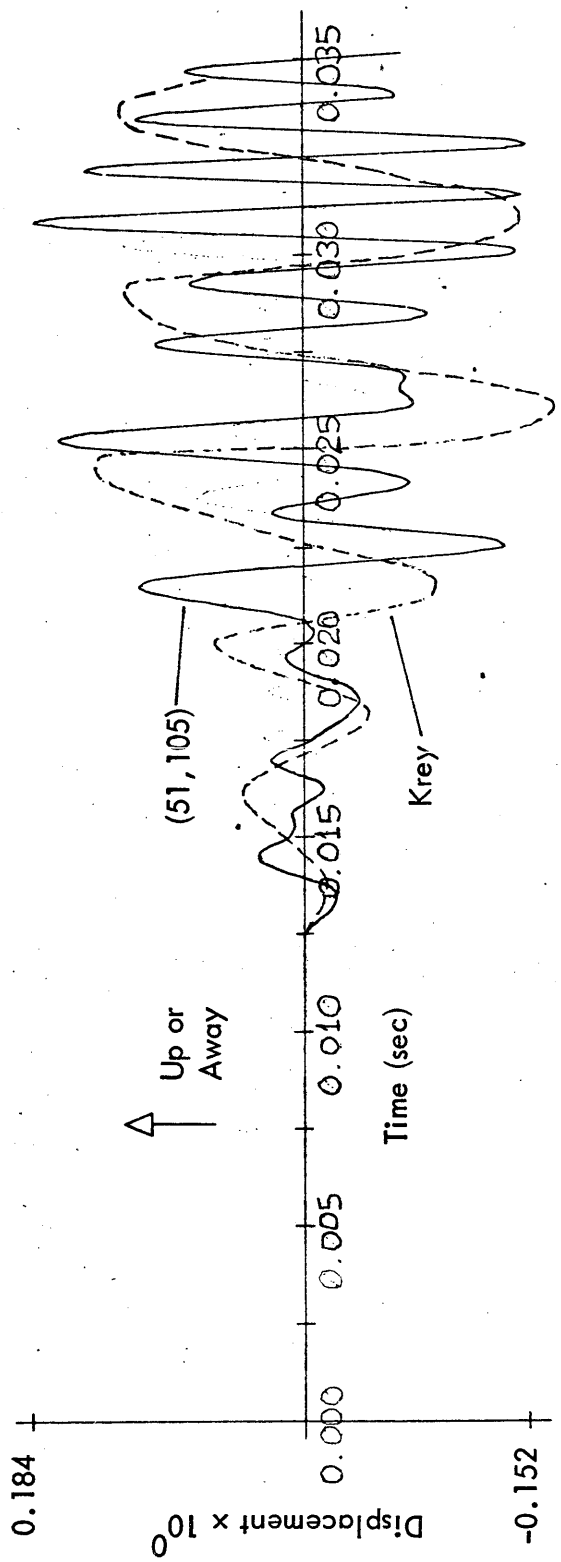

Figure 33. Radial displacement in the coal seam (depth = 31.2 m) at a distance of 20 m from the axis of symmetry, with a field recording from Krey (1963) superimposed.

direction. The source was a hammer.

The comparison is necessarily crude; Krey's seam is 2/3 the thickness of the modeled seam, his source was a hammer, and his recordings were made with geophones that have a limited dynamic range. The output would be further modified by the recording amplifier system. His geophones are, in addition, velocity transducers. The displacements calculated by FDNL.F10 have a dynamic range limited only by the computer word length, with no distortion related to damping, and no distortion in amplification.

Despite these drawbacks, Krey's trace and the model output have some correlation; there is a rough match at the beginning of both traces, and both develope their high amplitude channel wave at about the same time. A big difference is the higher frequency of waves in the model, particularly between 30 and 35 ms. There are several possible explanations for this. The hammer which Krey used may not have excited the high frequencies, whereas the source in the model had a peak excitation at 500 hz. The geophones and recording system of Krey may not have been able to handle high frequencies which may have been present, as most commercial systems have difficulty with frequencies greater than 300 hz. Even on records Krey made with dynamite there do not seem to be any periods less than 3.5 ms. In an effort to enhance the longer periods in the model output a simple filter was applied by performing a cumulative sum of the radial displacement at every time increment. The result is shown in figure 34, along with the superimposed trace from Krey. Since integration in the time domain has the effect of dividing by a constant proportional to frequency in the frequency domain, the lower frequencies should be enhanced by a factor of 6 db/octave. Figure 34 indicates a better correlation of the two traces as these higher frequencies are attenuated.

In figure 35, a second summation was performed, and it theoretically should enhance the lower frequencies by a factor of 12 db/octave. This figure shows a good correlation between 17 and 27 ms, with Krey's trace having a

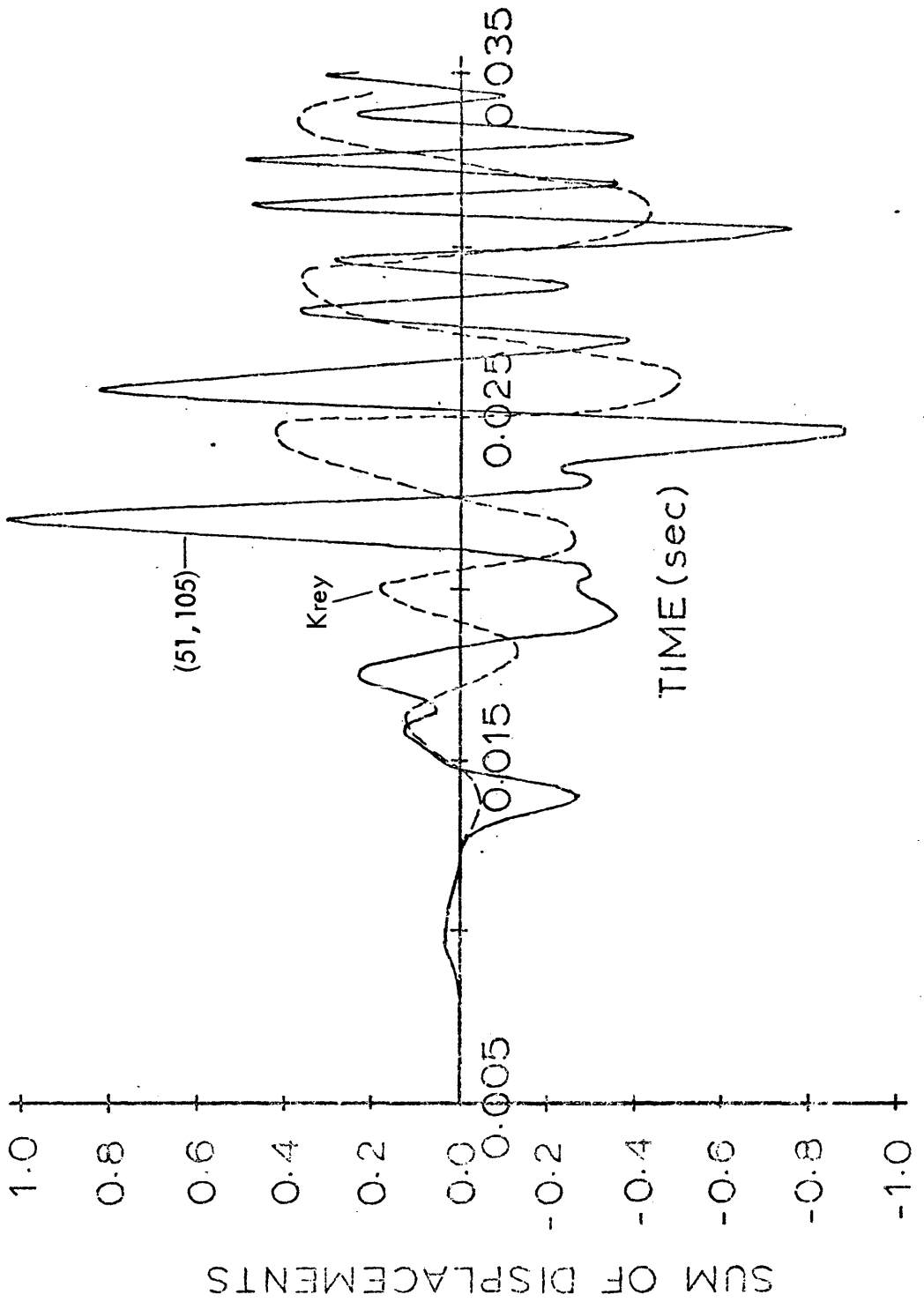

Figure 34. Cumulative sum of the radial displacement in figure 33, with a field recording from Krey (1963) superimposed.

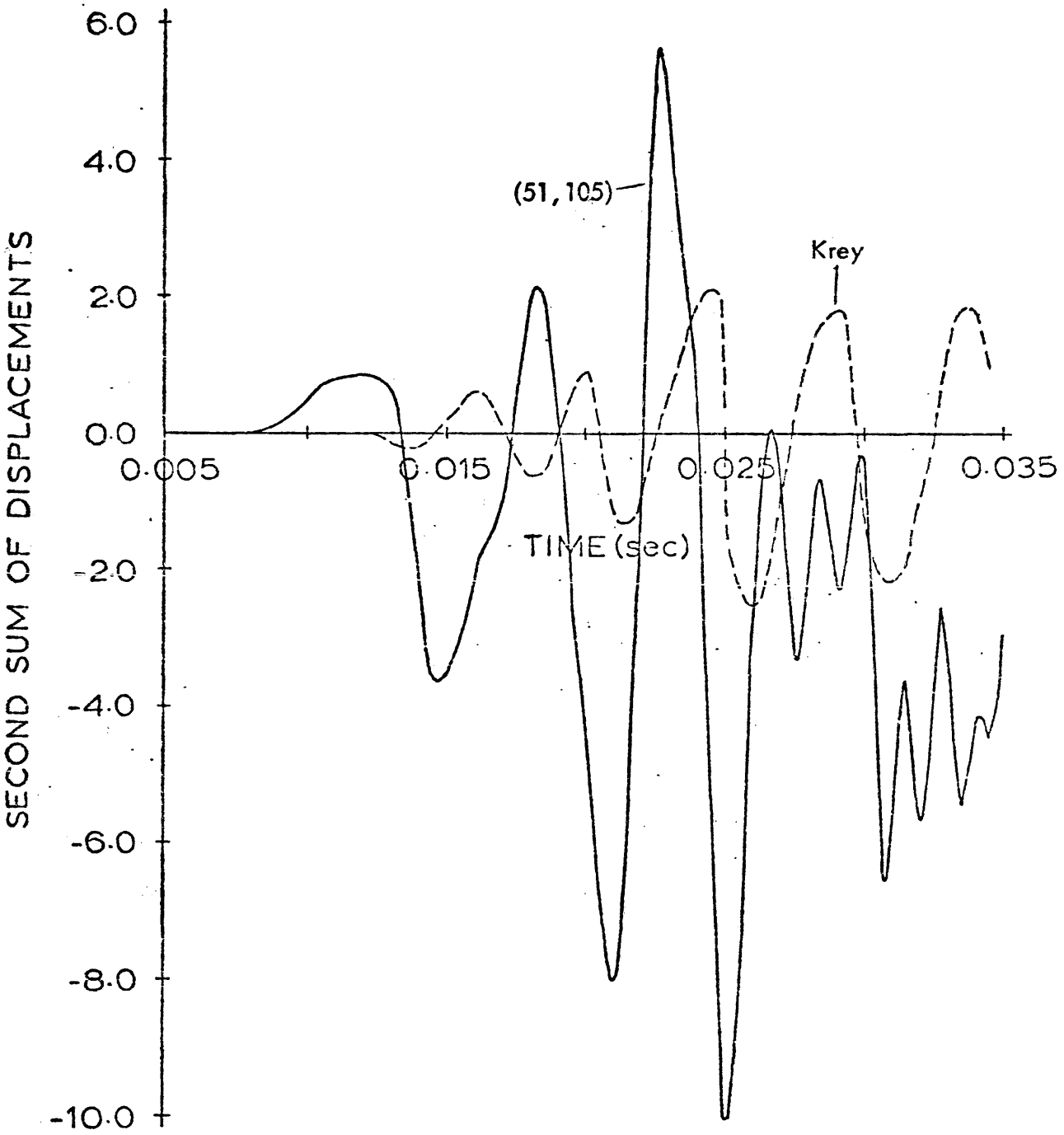

Figure 35. Second cumulative sum of the radial displacement in figure 33, with a field recording from Krey (1963) superimposed.

slight lag.

Although there is little of the channel wave to work with, some comparisons can be made with Krey's theory.

The large pulse at 21.4 ms on figure 22c (20 m from the source), and at 33.5 ms on figure 22d (30 m from the source), seems to be the most easily correlatable part of the channel wave on two successive records. As these geophones are 10 m apart, these times imply a velocity of 826 m/sec. The phase period is 2 ms, yielding a wavelength of 1.6 m. This point is marked by a cross in figure 32. It is not a good fit to Krey's dispersion curve, but one might consider it close in view of the fact that we are using far-field theory relatively near to the source. If a group period of 4.5 ms is taken from figure 35, at the same velocity, one arrives at a wavelength of 3.7 m. This point is also marked with a cross in figure 32. From Krey's group velocity curve for the second mode, a wavelength of 3.2 m would be predicted. As a note, the mature second mode Airy phase theoretically requires 40 ms to travel 20 m, and perhaps should not expected in figures 22c and 22d.

It is questionable whether first mode phenomena should even be looked for. As mentioned in the model description, the projected wavelength of the Airy phase is 15 m. Since at 30 m only part of the channel wave is recorded, and none at 40 m, it is necessary to look for this phase within two wavelengths of the source. It may be optimistic to expect any real developement at this short distance. However, with determination, almost anything can be found. If the reader looks at figure 35, it is possible to see a wave with a period of 8 to 9 ms. The first trough is at approximately 23 ms, the first peak at 28 ms, and the second trough at 33 ms. It appears to be superimposed on the trough of a wave with a period approaching 50 ms. If an approximate period of 10 ms and an approximate velocity of 1 m/ms is accepted, then a wavelength of 10 m is obtained. This point is marked with a cross on figure 32. In view of the fact that Krey's group velocity minimum is so flat, and that the source has a

high frequency skew, this is not an unreasonable figure.

A note which may be made concerning Krey's dispersion curves (Figure 32), is that the first mode phase velocity does not appear to be assymptotic to the shear velocity of the coal (v_s'). It should be so, if it is to be at all in accordance with the mode theory of boundary waves.

REVIEW

Validity of Program Output

Preliminary testing and comparisons to previous work indicated that the program did obtain correct results from the trial models. One of the runs was a case in which a low velocity layer was sandwiched between two high velocity layers, and since this is directly analogous to the coal seam model it should lend very strong credence to the results obtained.

A minor check on the output was made by situating two pairs of geophones symmetrically above and below the coal seam. These geophones should have measured the same (or mirror image) displacements until reflections arrived from the top and bottom of the model, which have dissimilar boundaries. The comparison of displacements gave a near-exact match.

Comparing the output to Krey's (1963) theory was a less definite matter. A fair match was obtained by comparing the strong first phase arrival of the channel wave to the dispersion curve for the second mode phase velocity. Longer period wave groups were identified by a simple filtering process, and a value was obtained which fell moderately close to Krey's group velocity dispersion curve for the second mode. The limited amount of output made velocity determinations crude. First mode analysis was complicated by the proximity of the source and the short length of the records. Filtering did, in the face of this, indicate the presence of a phenomenon with a period approximating 10 ms. The rather arbitrary assignment of a 1000 m/sec velocity yielded a wavelength of 10 m, and this point plotted close to the Airy phase on Krey's dispersion curve for the first mode group velocity.

A comparison of the output 20 m from the source with data recorded by Krey (1963) gave a reasonable match, after filtering, in that strong arrivals came at the same time and with the same general shape. The strongest differences were the ringing of the recorded waves, and the absence of any high

frequencies (greater than 300 hz) in the recorded data.

These observations do not contradict Krey's theory, but they can neither be regarded as strong supporting evidence. The most that can be said is that if Krey's theory is wrong, it is at least close.

The Strong Character of the Channel Wave

Figure 43 should be regarded as definitive evidence that at 20 m from the source a very significant proportion of energy is trapped within the coal seam. Radial displacement within the seam dwarfs anything else on the record. At 30 m there is less data to work with, but there is the same tendency.

So much energy seemed to be retained that a study was made to investigate the possibility that amplitude of displacement fell off as the square root of the distance from the source. Although any definite conclusion must again be hedged because of the limited amount of data, figure 43 would indicate that a square-root-r law could indeed be the case. The importance of this relationship is hard to over-emphasize. This would mean that at 100 m there would be 100 times more energy than spherical divergence would dictate, and amplitudes would be 10 times greater. At 1000 m amplitudes would be increased by a factor of 100. The square-root-r theory is viable.

The Directional Nature of Channel Wave Displacement

Almost all calculations and statements made with regard to channel waves have been based on the plots of radial displacement. The radial displacement near the center of the seam is generally quite a bit larger than the vertical, and often there is no sign at all of important phases in the vertical displacement plots. This leaves it an open question as to where and what the maximum vertical displacement in the seam really is.

CONCLUSIONS

It can be stated, with no question, that the impulsive point source in the coal seam caused a strong channel wave to be generated. The channel wave maintained a strong amplitude to a distance of at least 30 m from the source. Radial displacements in the center of the coal seam exceeded radial displacements in the shale 0.3 m above the coal by more than an order of magnitude. There is evidence to suggest that energy in the channel wave diverges cylindrically, rather than spherically, which would imply that the amplitude of the channel wave decreases only as the square-root of its distance from the source.

This thesis supports the concept that a low-velocity coal seam in competent country rock can effectively trap energy, and that it is worthwhile to investigate the possibility of locating discontinuities by detecting dispersions or reflections of channel wave energy.

RECOMMENDATIONS FOR FUTURE WORK

There are several clearly defined areas in which the work presented here should be continued. The most critical improvements would be a larger model (in radial extent) and a much longer time history of displacements. If the bulk of the channel wave could have been observed at all of the geophones, instead of only two, a great deal more could have been said even for the restricted model considered here. And if the wave could have been observed 300 m from the source as well as at 30 m, definite statements could be made about a root-r law. The last suggestion would cause, however, a two-orders-of-magnitude increase in the expense of running the finite difference program.

Another important contribution would be made if amplitudes were assigned to the rays of body waves that were investigated. It would be a quantum step in understanding channel waves if they could be described in terms of ray theory. An immediate dividend would be the obsolescence of the need to use expensive finite difference or finite element techniques to study channel wave phenomena.

Finally, it would be advisable to place geophones in a vertical string across the seam. This would cescribe the distribution of vertical displacements due to the channel wave.

REFERENCES

Alterman, Z., and Karal, F. C., 1968, Propagation of elastic waves in layered media by finite difference methods: Seismol. Soc. of America Bull., v. 58, no. 1, p. 367-397.

Alterman, Z., and Karal, F. C., 1969, Errata to "Propagation of elastic waves in layered media by finite difference methods": Seismol. Soc. of America Bull., v. 59, no. 1, p. 471.

Krey, T. C., 1963, Channel waves as a tool of applied geophysics in coal mining: Geophysics, v. 28, no. 5, p. 701-714.

Leitinger, H., 1969, Investigation of displacement steps in a layered half-space by the finite difference method: Colorado School of Mines Doctoral Thesis.

Lysmer, J., and Kuhlemeyer, R.L., 1969, Finite dynamic model for infinite media: Journal of the Engineering Mechanics Division, ASCE, v. 95, no. EM4, p. 859-877.

Oden, J. T., 1972, Finite elements of nonlinear continua: McGraw-Hill Co., New York.

Schwaitzer, T., 1965, Geophysical studies of the continuity of coal seams: International Journal of Rock Mechanics and Mining Sciences, vol. 2, p. 167-196.

Sharpe, J. A., 1942, The production of elastic waves by explosion pressure: Geophysics, vol. 7, no. 2.